Contents lists available at ScienceDirect

# Materials Today Communications

journal homepage: www.elsevier.com/locate/mtcomm

# Alendronate reinforced polycaprolactone-gelatin-graphene oxide: A promising nanofibrous scaffolds with controlled drug release

Hendrik Setia Budi [a], Alla Davidyants [b], Mohammad Rudiansyah [c], Mohammad Javed Ansari [d], Wanich Suksatan [e], Mohammed Q. Sultan [f], Abduladheem Turki Jalil [g,1], Milad Kazemnejadi [h,*]

[a] *Department of Oral Biology, Faculty of Dental Medicine, Universitas Airlangga, Surabaya 60132, Indonesia*
[b] *Department of Propaedeutics of Dental Diseases, Sechenov First Moscow State Medical University, Moscow, Russia*
[c] *Division of Nephrology & Hypertension, Department of Internal Medicine, Faculty of Medicine, Universitas Lambung Mangkurat / Ulin Hospital, Banjarmasin, Indonesia*
[d] *Department of Pharmaceutics, College of Pharmacy, Prince Sattam Bin Abdulaziz University, Al-kharj, Saudi Arabia*
[e] *Faculty of Nursing, HRH Princess Chulabhorn College of Medical Science, Chulabhorn Royal Academy, Bangkok 10210, Thailand*
[f] *College of Dentistry, Al-Ayen University, Thi-Qar, Iraq*
[g] *Medical Laboratories Techniques Department , Al-Mustaqbal University College, Babylon, Hilla, 51001, Iraq.*
[h] *Department of Chemistry, Faculty of Science, Golestan University, Gorgan, Iran*

## ARTICLE INFO

## ABSTRACT

Graphene oxide-reinforced electrospun scaffolds have attracted the attention of many researchers to be served in biomedical applications such as tissue engineering and drug delivery. In this study, the nanofibrous scaffolds were fabricated from polycaprolactone (PCL), gelatin (Gel) and modified-graphene oxide nanoparticles (GO NPs) to investigate their possible application in bone tissue engineering. Alendronate (Ald.), as a bisphosphonate drug, was immobilized covalently (Gel/PCL-GO-Ald.) and non-covalently (Gel/PCL-GO*Ald.) on the modified GO surface. The modified GO NPs were characterized by FTIR, XRD, XPS, FESEM, TEM, and HRTEM analyses. The incorporation of GO in the nanofibrous scaffolds improves the electrical conductivity, swellability, and mechanical strength of the fibers, which were investigated in this work. *In vitro* drug delivery of alendronate on both Gel/PCL-GO-Ald. and Gel/PCL-GO*Ald., as a drug delivery model, were examined based on a colorimetric assay. Gel/PCL-GO-Ald. hybrid nanofibers revealed good biocompatibility in the presence of human osteosarcoma cells, and no trace of cellular toxicity was observed. Cell culture was monitored by FESEM, XRD (before and after cell culture), and fluorescence analyses, which showed that the cells grown on the scaffolds exhibited a spindle-like and broad morphology, and covered almost the entire fibrous surface uniformly. The scaffolds showed antibacterial activity against *E. Coli* and *S. aureus* bacterial strains. Toxicity and biocompatibility of the scaffolds were investigated by MTT analysis. The response of the scaffolds to hemolysis of red blood cells was also studied.

## 1. Introduction

In recent years, with the preparation and construction of polymer-based scaffolds, a suitable alternative to repair or improve the function of damaged tissues with the help of tissue engineering has been proposed. Scaffolds made from electrospun polymer nanofibers are interesting due to their porous three-dimensional structure at the nanoscale, which can simulate the chemical and physical structure of the extracellular matrix (ECM) of the human body [1,2].

The choice of engineering polymers for use in bone tissue engineering should be such that not only provides the suitable interaction between the various fiber components, but also the resulting nanocomposite should have minimal toxicity, high antibacterial activity, good electrical conductivity, and high hydrophilicity [1–4]. PCL, as a fully biodegradable and non-toxic polymer, is one of the popular candidate for the preparation of scaffolds used in bone tissue engineering [5]. Kim et al. [6] investigated the mechanical properties of PCL-coated porous hydroxyapatite (HA) scaffolds and the release of tetracycline hydrochloride from the scaffolds for application in bone tissue engineering. Khodir et al. [5] immobilized tetracycline hydrochloride on PCL/chitosan composite scaffolds with high mechanical strength and controlled drug release, which improves ossification

---

* Corresponding author.
  *E-mail address:* miladkazemnejad@yahoo.com (M. Kazemnejadi).
1 https://orcid.org/0000-0001-8403-7465

properties in tissue engineering applications.

However, PCL has disadvantages such as low hydrophilicity, low mechanical strength, inability to function properly with drug molecules, and low electrical conductivity, which limits its use in many tissue engineering applications. Gelatin is a solid biopolymer made by hydrolyzing collagen in connective tissue or animal bones. Gelatin has several advantages such as biodegradability, cost effectiveness compared to synthetic polymers, lack of antigen formation, high biocompatibility, high *in vivo* swelling, cell migration, accelerated adhesion, and the formation of polyelectrolyte complex ability [2,7]. Nanofibers made from gelatin, like collagen fibers, are cost- effective and also have biological properties, that enhance the performance of immune system. One of the main problems of gelatin is its dissolution at temperatures above 37 °C. For this reason, gelatin is combined with a synthetic polymer (like PCL) to preserve the shape and structure of the fibers. Due to the similarity of gelatin with collagen, electrospinning of gelatin with other synthetic polymers has attracted much attention in bone tissue engineering [2].

On the other hand, targeted and controlled delivery of drugs with high side effects is also one of the important tasks of prepared scaffolds for application in tissue engineering and should be in a way that minimizes the side effects associated with drugs. For example, Ald. is one of these drugs, that its high doses cause severe side effects due to irritation of the upper gastrointestinal tract, which severely limits its use in drug delivery [8,9]. Bisphosphonates (BPs) are potential antiresorptive drugs that their use in the metabolic bone diseases treatment has been well known [10–12]. Ald. is one of the most potent nitrogenous BPs drug in the treatment of diseases such as osteoporosis, Paget's disease as well as hypercalcemia of malignancy [8], and commonly used to treat osteoporosis [13,14]. The previous reports have shown that Ald. enhances mesenchymal stem cells (MSCs) and osteogenesis of osteoblasts [10]. Ald. inhibits the activity of osteoclasts *via* farnesyl diphosphate synthase suppression, causing calcium salts to remain inside the bone and reducing the process of osteoporosis [14]. Previous studies have shown that Ald. stimulates the differentiation of osteoblasts and proliferation in human bone marrow-derived MSCs [10]. Very recently, the same results were also obtained by Shi et al. using Ald. crosslinked chitosan/poly-caprolactone scaffold for osteogenic differentiation *in vitro* and new bone formation *in vivo* in rats with a critical-sized calvarial defect [15]. In another report, it was shown that locally implanted Ald. causes bone formation in a critical-sized calvarial defect model in mice [16]. However, its high solubility in aqueous media (due to its high hydrophilic nature) as well as in high doses leads to side effects and therefore in order to be used in bone tissue engineering, it requires controlled release through scaffolds with a convenient design. Therefore, by designing a drug delivery system with a very slow and controlled release, this valuable drug can be used in bone tissue engineering. Recently, Rumian et al., loaded sodium alendronate on poly(L-lactideco-glycolide) microparticles and then immobilized them on ceramic scaffolds for treatment of the bone defects [17]. The prolonged release of Ald. showed that 10–100 μg/mL of Ald. is toxic to osteoblasts, while 5 and 2.5 μg/mL concentrations did not hamper osteoblasts viability. Previously, the cytotoxicity of sodium alendronate immobilized on solid lipid nanoparticles to A549 cells showed a low toxicity associated with alendronate at 70–85% drug loading [18].

Due to the high surface-to-volume ratio of NPs, the drug molecules can be immobilized on their surface at high loading rates. Also, reinforcement of nanofibrous scaffolds with NPs causes controlled and targeted drug release in the physiological environment, as well as improvement of electrical conductivity, mechanical strength, and even hydrophilicity of the scaffold for use in tissue engineering [19]. Graphene-based nanofibers, based on the number of layers, dimensions, and chemical modifications provide good interactions with biomolecules, cells, and tissues [20,21]. The high aspect ratio associated with GO NPs promotes cellular interactions. Drug molecules can be loaded on the GO surface *via* covalent, ionic, or π-π stacking, resulting in controlled release of a drug into the physiological environment [22].

Studies have shown that GO can bind to- and proliferate bone and mesenchymal stem cells [23]. It has also been shown that GO can enhance the differentiation of bone stem cells due to their remarkable mechanical properties [23]. Luo et al. fabricated the electrospun PLGA /GO nanofibers with improved bone cell proliferation properties [24]. Based on their results, examination of cytotoxicity results after 1, 2 and 3 days showed that the cell growth rate with GO increased significantly compared to GO-free nanofibers. This improved cell growth was attributed to the ability of proteins that can be adsorbed onto the surface of the GO-loaded scaffold.

In the last decade, the application of scaffolds made of nanomaterials-reinforced Gel/PCL nanofibers in bone tissue engineering has been extensively investigated [25], and in most studies, nanofibers have shown a successful effect on bone tissue healing [25,26]. Previously, Heidari et al. studied the application of tetracycline hydrochloride (TCH)-loaded PCL/Gel/GO nanofibers for use in nerve tissue engineering, in which the π-π stacking interaction between TCH and GO, controls the release of TCH [27]. Recently, the application of GO (1% w/w)-reinforced PCL/Gel nanofibrous scaffolds has been evaluated in cardiac tissue engineering [28]. Also, Kashte et al. reported the synergistic effect of GO and *Cissus quadrangularis* (CQ) on the layer-by-layer herbal cell PCL-GO-CQ scaffold for bone tissue engineering [29]. PCL nanofibrous scaffolds containing Sr/Se-hydroxyapatite/GO [22], gelatin-polycaprolactone-nanohydroxyapatite [2], *in-situ* polymerized polypyrrole nanoparticles immobilized PCL [4], and PCL scaffolds enriched with vitamin D3 -loaded LDH [30], were some of the recent advancements in the use of PCL based-scaffolds in bone tissue engineering.

Very recently, the PCL/Gel antibacterial scaffolds reinforced by dicalcium phosphate (DCP)-modified GO with controlled release of clindamycin were developed for possible application in bone tissue engineering [25]. In this paper, the fabrication of nanofiber hybrid scaffolds using PCL synthetic polymer, gelatin natural polymer along with GO modified by alendronate sodium trihydrate, was investigated. The application of the obtained scaffolds was evaluated for possible use in bone tissue engineering as well as controlled release of alendronate drug. The scaffolds were made by electrospinning method, which in the final scaffold, both polymer components were in the form of separate fibers and have created a cohesive and intertwined structure. Gelatin, despite having desirable biological properties, does not have good mechanical strength in the body environment; Therefore, its combination with PCL has been used. Alendronate is also a bisphosphonate drug that, despite its many medicinal properties, requires very slow release. In this way, GO NPs were functionalized to control release of Ald., and then used to prepare nanofibers.

## 2. Experimental

### 2.1. Materials

Alendronate sodium trihydrate was purchased from selleckchem company (Bioactive compounds expert). 3-(4,5-Dimethylthiazol-2-yl)−2,5-diphenyltetrazolium bromide was provided from Sigma Aldrich for MTT test. Gelatin Type B (from bovine skin) was purchased from Sigma. High surface area GO NPs containing 9.4 wt% O and 90.6 wt% C, with a thickness of 1.0 nm, a lateral size of 0.2–10 μm, and a 400 $m^2$/g surface area was provided from ACS MATERIAL Co. (Advanced Chemicals Supplier). PCL 90000 g/mol (white pellet, melting point: 58–60 °C) was purchased from Shenzhen Esun Industrial Co., Ltd., China. A standard tetracycline disk (30 μg) was supplied from Fluka (75,141, yellow disk). All solvents had an analytical grade with > 99% purity and were dried before use.
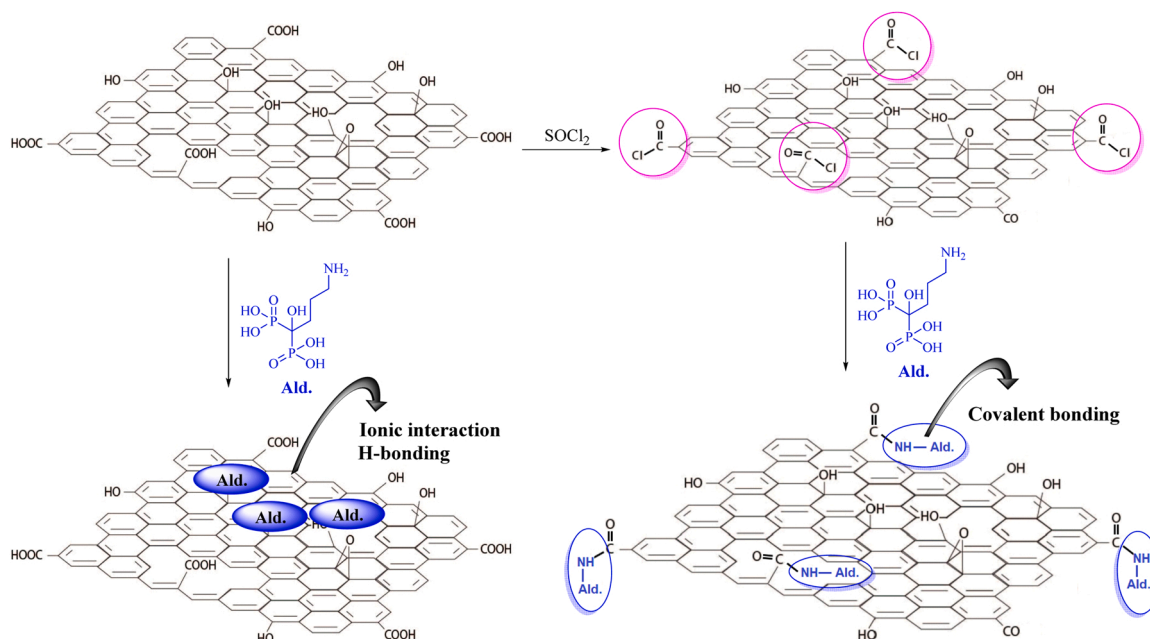
**Scheme 1.** Surface modification of GO by alendronate sodium trihydrate.

## 2.2. Graphene oxide functionalization

### 2.2.1. Surface modification of graphene oxide by thionyl chloride (SOCl₂)

Chlorine-functionalized GO was synthesized according to a procedure reported elsewhere [25,31]. 2.0 g of GO was added to 25.0 mL of SOCl₂ in a canonical flask. The mixture was stirred for 1 h at room temperature, then refluxed for one day. In the next step, the mixture was cooled to ambient temperature and the remaining (unreacted) SOCl₂ was removed under reduced pressure. The desired product (GO-Cl NPs) was centrifuged, dried in vacuum at 90 °C, and stored in a P₂O₅ powder containing-vacuum desiccator (Scheme 1).

### 2.2.2. Surface modification of GO by alendronate sodium trihydrate

Surface modification of GO by alendronate was performed by covalent as well as ionic/H- bonding (Scheme 1). In covalent bonding, chlorine-functionalized GO (1.0 g) was dispersed in dimethyl sulfoxide (DMSO, 20 mL), and then alendronate sodium trihydrate (0.2 g), and triethanolamine (2.0 mmol) was added to the mixture, and the mixture was refluxed for 8 h. The mixture was then cooled and the GO-Ald. was separated by centrifugation, washed with deionized water and EtOH, then dried and stored in vacuum.

For ionic functionalization of alendronate on GO (Scheme 1), GO (1.0 g) was dispersed in 20 mL of DMSO, then alendronate sodium trihydrate (0.2 g) dissolved in DMSO (2.5 mL) was added dropwise to the mixture during 30 min (The addition was done under ultra-sonication). Then, the mixture was stirred at room temperature for 8 h. The resulting GO*Ald. was centrifuged, washed with deionized water and EtOH, then dried and stored in vacuum.

## 2.3. Preparation of Gel/ PCL, Gel/PCL-GO, and Gel/PCL-GO hybrid nanofibers by electrospinning of their solutions

Electrospun preparation of the nanofibers was performed on a Fluidnatek LE-100 instrument from electrospinning Fluidnatek company equipped with two syringe pump that can be injected from both sides and each pump can inject three polymer solutions. In first, two solutions of PCL in dimethyl carbonate (14% w/v), and gelatin in 90% acetic acid (15% w/v) were prepared. The solutions were poured into the syringes after 12 h of stirring. The Gel: PCL mixture was electrospun at a ratio of 50:50, so that PCL was spun in one syringe and gelatin from another

syringe to prepare the desired hybrid nanofiber [25].

A same procedure was also applied for the preparation of Gel/PCL-GO, in which GO 2.5 wt% was sonicated for 1 h in dimethyl carbonate. At last, the PCL polymer mixture was added to the dispersed GO and the resulting solution was stirred for another 1 h. Finally, to produce the desire Gel/ PCL-GO nanofibers, PCL-GO solution on one side and gelatin polymer solution on the other side were electrospun.

Preparation of Gel /PCL-GO nanofiber scaffolds reinforced by covalent- and noncovalent- bonded alendronate was also performed according the mentioned procedure.

## 2.4. Physiochemical characterization of nanofibrous scaffolds

### 2.4.1. Electrical conductivity measurement of the nanofiber scaffolds

The electrical conductivity of the scaffolds was determined using a Galvanostat - Potentiostat Autolab, PGStat 302 N model equipped with two electrodes (from Metrohm Autolab company) in the range of 0.001–10⁶ Hz. For electrical conductivity measurements, the nanofibers were cut into 0.9 × 0.9 cm² species and using Eq. (1), the resistance (in ohms) and the electrical conductivity (in µS /cm) of the nanofibers were measured [32,33].

$$EC = \frac{L \times 10^4}{A \times R} \tag{1}$$

Where EC is the electrical conductivity in µS/cm, R is the impedance in Ω, A is the surface area of the nanofiber, and L is the thickness of the nanofiber. The thickness (L) of the nanofibers was measured with a UK-made Shirley thickness gauge. In first, the electrical resistance (R) curves against length of the nanofiber scaffolds (L) were plotted and the resulting slope was resistivity (ρ) (ESI, Fig. S1a-d). The electrical resistivity denoted by ρ (in Ωm) was obtained by Eq. (2):

$$\rho = \frac{RA}{L} \tag{2}$$

### 2.4.2. Evaluation of mechanical properties of the nanofiber scaffolds

The mechanical properties of the scaffolds were studied using a INSTRON 5566 UTM (UK) instrument in accordance with the ASTM D638 (tensile test). In this way, the scaffolds were prepared using pre-prepared molds according to a standard shape. The nanofibers were

cut into equal rectangular shapes with 10–60 mm in dimensions, and then placed between two jaws with a distance of 15 cm [34]. Using a digital caliper (NEIKO 01407 A), the samples thickness was determined from three different areas of the nanofibers. The tensile test was then performed at 5 mm/min speed (until failure) at room temperature. A load cell of 50 N was used for this experiment.

### 2.4.3. Swelling measurements of the nanofibers

The swelling amount of a film could be calculated in two different ways, including (i) calculating changes in film volume before and after swelling [35] and (ii) calculating changes in film weight in solvents [36]. The swelling volume of the nanofibers (in mL/g) was calculated by changing the weight of the film using Eq. 3 [37]:

$$V_s = \frac{W_2 - W_1}{W_1} \times \frac{1}{d_s} \qquad (3)$$

Where $V_s$, $W_2$, $W_1$, and $d_s$ are the nanofiber swelling in mL/g, the swollen network weight in gr, the weight of dry nanofiber in gr, and the PBS buffer density (solvent), respectively.

In practice, the dry nanofibers were weighted to obtain $W_1$ and then immersed in PBS at room temperature for 5 h to determine $W_2$. In order to weigh the swollen scaffold in the PBS, it was first removed from the solution by forceps, and weighed after a few seconds to drip excess droplets from the surface of the scaffold [38].

### 2.5. Determination of alendronate concentration and release

To study the release behavior of alendronate from the nanofibers, phosphate buffer was used as the acceptor phase (release medium) *in vitro* [39]. To investigate the release of alendronate from Gel/PCL-GO-Ald. and Gel/PCL-GO*Ald. nanofibers under physiological conditions, a certain weight of nanofibers was added to 10 mL of phosphate buffer at pH 7.4 at 37 °C under constant shaking. To determine the amount of alendronate released from the nanofibers, the sample was completely removed from the medium at various time intervals, and added to fresh phosphate buffer solution [40]. The amount of alendronate was determined using a fast and sensitive colorimetric method reported by Sun et al. based on $Ce^{4+}$ triggered oxidation of 3,3′, 5,5′-tetramethylbenzidine (TMB) [41]. The optical absorptions were performed using a SPECORD 210 PLUS Analytikjena spectrophotometer. This test was repeated for three days and three times per day. In this method, TMB produces a blue oxidation product (oxTMB) in the presence of $Ce^{4+}$ and in the absence of any oxidant. In the presence of Ald., due to the redox reaction between $Ce^{4+}$ and Ald., the oxidation capacity of $Ce^{4+}$ is greatly reduced. Thus, based on the oxTMB absorption intensity at 652 nm, the amount of Ald. was measured in the solution. oxTMB has a blue color that changes to pale blue in the presence of Ald.

The response of $Ce^{4+}$–TMB system to Ald. concentration was investigated by UV-Vis. technique at $\lambda_{max} =$ 652 nm (Fig. S2a). The absorption intensities of the $Ce^{4+}$–TMB system at 562 nm, decreases linearly with increasing of Ald. concentration, while the $\Delta A$ increases systematically. $\Delta A$ has linear response to the Ald. concentration in the concentration range of 0.1–10.0 μM and 10.0–60.0 μM, with the linear fitting equations of $\Delta A = 0.1149 + 0.04111\ C_{ALd.}$ (μM) ($R^2 = 0.9938$) and $\Delta A = 0.3389 + 0.02020\ C_{ALd.}$ (μM) ($R^2 = 0.9939$), respectively (Fig. S2b).

To prepare 1 liter of phosphate buffer, potassium chloride (0.2 g), sodium chloride (8.0 g), potassium dihydrogen sulfate (0.24 g), and sodium hydrogen phosphate (44.1 g) were dissolved in 800 mL of distilled water. The solution pH was adjusted to 7.4 by addition of 1 M NaOH or 1 M HCl, and then the volume of the solution reached to 1 L [42].

### 2.6. Cells culture on the scaffolds to study cell morphology

100,000 cells were cultured on the scaffolds. Prior to cell culture, the scaffolds were maintained in DMEM (Dulbecco modified Eagle medium) medium with 100 international units per mL of penicillin, 10% FBS fetal serum, and streptocin. The scaffolds were sterilized under UV light, then placed in a cell-free culture medium (in polystyrene -dishes) for 8 h. Then, 1 mL of cell suspension containing 100,000 cells was poured into each well and the culture dishes were incubated for 5 days with 5% $CO_2$ and 95% humidity at 37 °C. Cell culture medium was frequently replaced with fresh medium [43]. In following, the suspension solution was removed from all wells and the samples were washed with PBS 1X. The cells were then treated with glutaraldehyde for 3 h. The samples were dehydrated for 15 min in 50%, 75%, 90% and 100% EtOH and then treated with hexamethyl disilazans, and dried. Finally, to evaluate the morphology of the cells, the completely dried samples were studied by SEM analysis.

Cell viability on the nanofibrous scaffolds was studied on a Trans-Detect® Cell LIVE/DEAD Viability/Cytotoxicity Detection Kit (China) for differentiation between living and dead cells by Calcein-AM (provided in the kit), and Propidium iodide (PI), respectively. This test was accomplished in accordance with the manufacturer's instructions, and the cells were observed using a fluorescence microscope. Cell viability was studied after 1 and 5 days of culture.

### 2.7. Disc diffusion test

The antibacterial activity of Gel/PCL, Gel/PCL-GO, Gel/PCL-GO-Ald., and Gel/PCL-GO*Ald. nanofibers was evaluated by the disk diffusion (DD) test against gram-negative *E. coli* and gram-positive *S. aureus* bacteria [44]. For this test, the disks with 5.0 mm in diameter from each of the nanofibers were punched by a sterile puncher and sterilized under UV light for 20 min.

Bacterial suspension with a concentration of 0.5 McFarland was used and spread out over the culture medium surface by a swap. The nanofiber discs were placed on the surface of the culture medium using sterile forceps and fixed on the medium with a small pressure. Then, the plates were incubated for a day at 37 °C. Gel/PCL nanofiber (without Ald. and GO) was used as a positive control in the test. The test was performed in three replications and a mean value was reported for the diameter of growth inhibition zone (in mm), which was measured using a digital caliper (NEIKO 01407 A). Also, a standard tetracycline disc was used for comparison.

### 2.8. MTT assay

To evaluate the cytotoxicity and biocompatibility of the nanoparticles, Saos-2; G-292 (Human osteosarcoma cell line) was provided from Pasteur Institute of Iran cell bank and cultured on Gel/PCL, Gel/PCL -GO, Gel /PCL-GO*Ald., and Gel /PCL-GO-Ald. scaffolds. The scaffolds were sterilized and stored in RPMI-1640 growth medium with 100 IU/mL streptocin, 10% fetal bovine serum (FBS), and penicillin before cell culture. Then, 1 mL of cell suspension containing 100,000 cells was added to each well. A well containing culture medium and scaffolds-free cells was considered as a control sample. The plates were incubated with 95% humidity and 5% $CO_2$ for 1, 2, and 3 days at 37 °C ($CO_2$ INCUBATOR NB-203 made by N-BioTek, INC). After incubation time, the grown cells were incubated for 4 h along with 20 μL of MTT dye (5 mg/mL). Then, 250 μL of DMSO was added to each well, which the yellow color of MTT powder turned purple. The plates were shaken for 15 min, then the obtained solution was transferred to the 96-Well ELISA Microplates. The samples (100 μL) was transferred to the wells and their absorption was read at 570 nm using a Synergy HT spectrometer (BioTek USA). The cell viability% was calculated using the following Eq. (4) [45–47]:
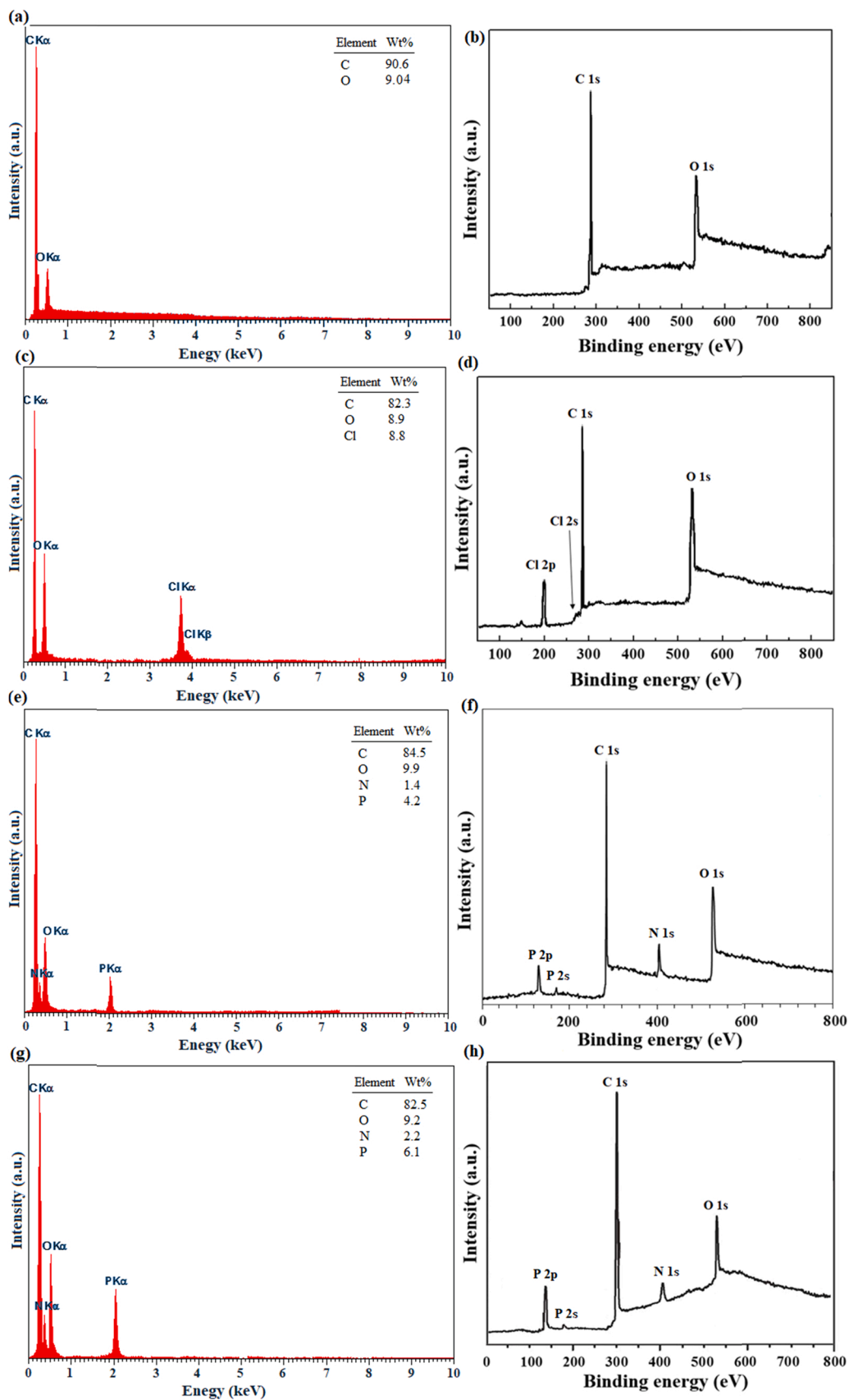
**Fig. 1.** EDX analyses (mean of 6 points) of (a) GO [25], (c) GO-Cl [25], (e) GO-Ald. (covalently bonded alendronate), (g) GO*Ald. (non-covalently bonded alendronate (*via* ionic/ H-bonding)). XPS overall survey (normalized, energy corrected) analyses of (b) GO, (d) GO-Cl, (f) GO-Ald., and (h) GO*Ald.
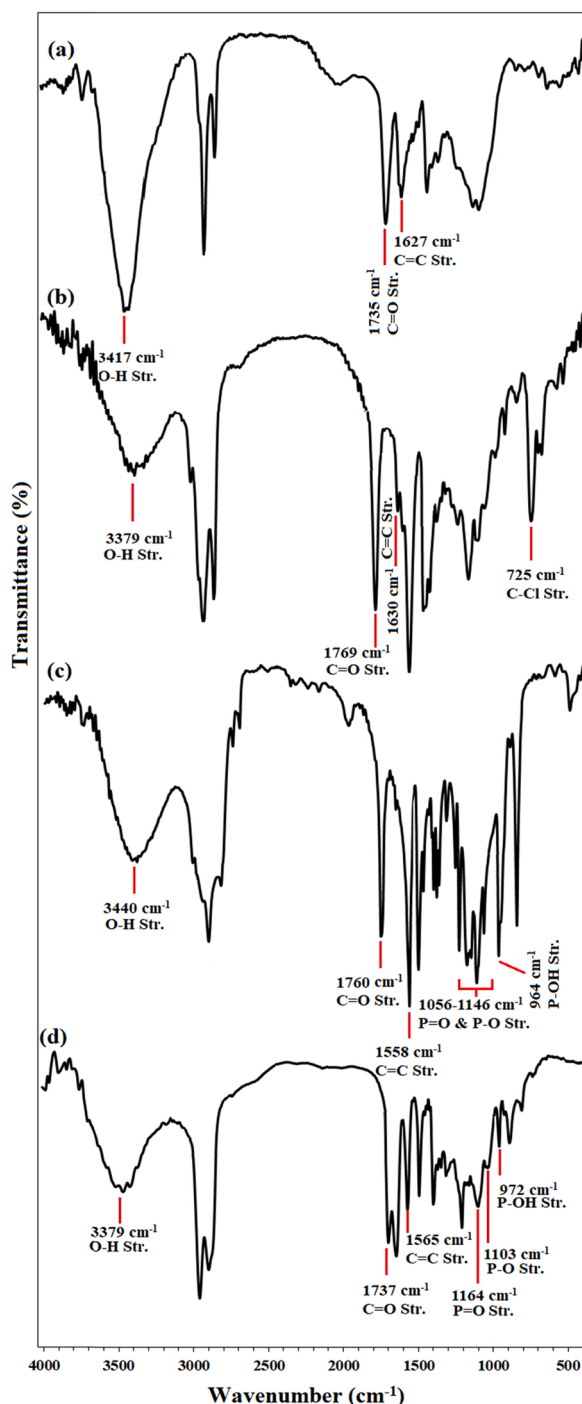
in a tube containing EDTA was centrifuged at 13000 rpm for 2 min to separate the red blood cells from the plasma, then washed three times with PBS buffer. Then, they were poured into separate microtubes, so that 100 million red blood cells were poured into the each microtube. The final volume in each sample was then increased to 1 mL using PBS at pH 7.4, and a punched piece of each of the nanofibers (0.5 cm in diameter) was added into the microtubes. The microtubes were incubated for 1 h at 37 °C. The tubes were then centrifuged at 5000 rpm for 5 min, and then the absorption of the supernatant was read at 540 nm. Erythrocytes treated with 1% Triton X-100 solution and buffer were used as a positive and negative control, respectively. Each test was repeated 3 times for each nanofiber and the results were reported as average [48].

## 3. Results and discussion

### 3.1. Studies over the characterization of modified GO

#### 3.1.1. Determination of Ald. loading on GO

The amount of alendronate loaded on GO was measured using the $Ce^{4+}$ triggered oxidation based on a method reported by Sun et al. [49]. This experiment was repeated three times on Gel/PCL-GO-Ald. and Gel/PCL-GO*Ald. scaffolds and mean values were reported. According to the results, the loading rate of Ald. on GO *via* covalent- and ionic/H-bonding was equal to 7.6 wt% and 10 wt%, respectively. Since 2.5 wt% of GO is added to the PCL polymer blends, therefore, the polymer blends contain 0.25 and 0.19 wt% of Ald. for ionic and covalent bonding, respectively.
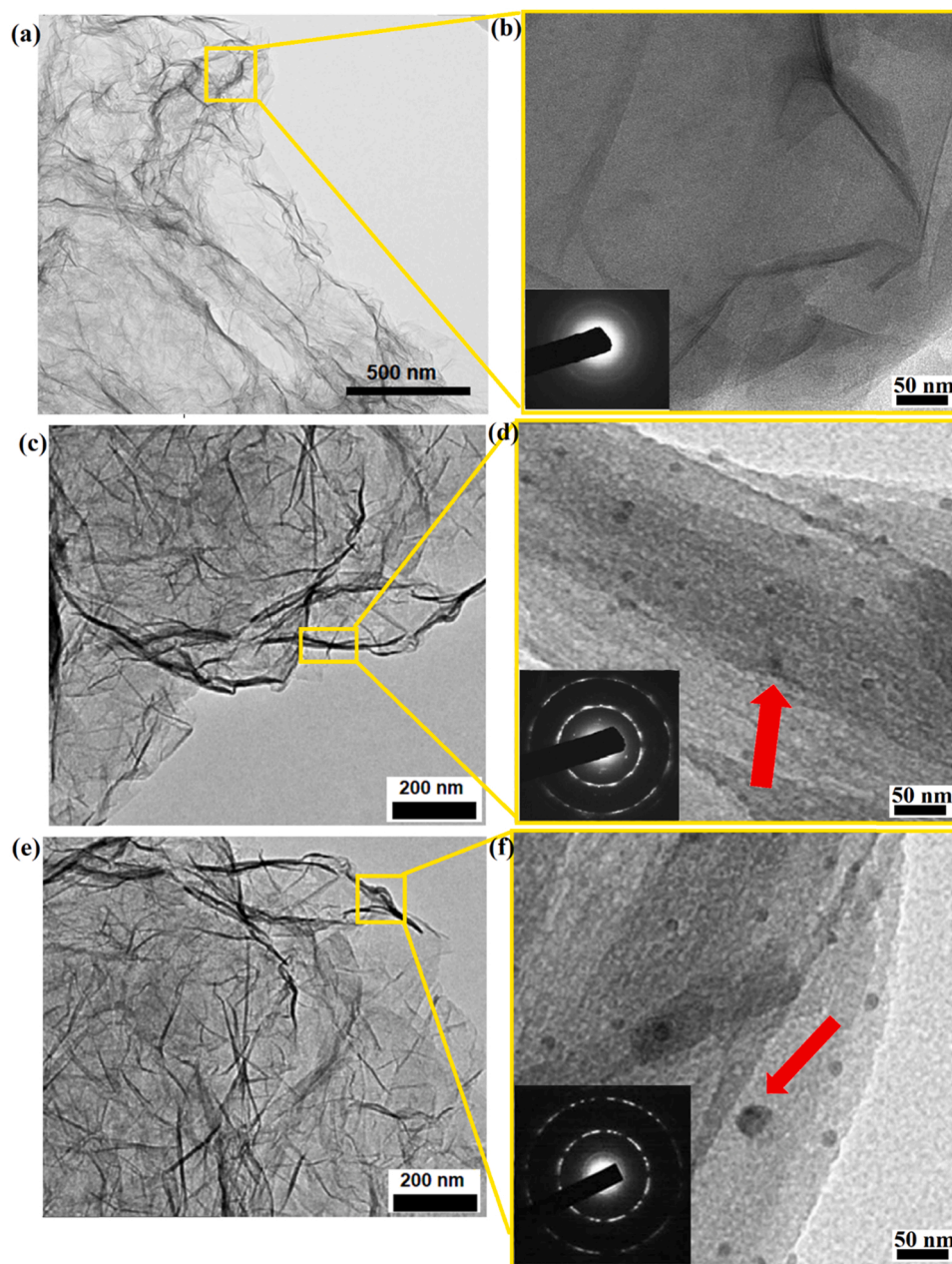
#### 3.1.2. EDX analysis

Energy dispersive X-ray (EDX) analysis of GO was conducted using a JEOL 7600 F FE-SEM, equipped with an energy dispersive X-ray spectrometer from Oxford Instruments. The findings were completely consistent with the EDX results (Fig. 1- a,c,e,g). The elemental analysis also proved the successful functionalization of GO surface with Cl and Ald. As shown in EDX spectrum of GO-Cl (Fig. 1c), the detection of Cl with 8.8 wt% confirmed the successful chlorination of GO. The presence of P and N elements in Ald. helped to detect its immobilization on GO (Fig. 1e,g). Removal of Cl element in the EDX spectrum of GO-Ald. (Fig. 1e) also confirmed that Ald. was immobilized on GO *via* the covalent bonding. Higher levels of P and N in GO*Ald. indicate higher loading of Ald. through ionic interactions compared to covalent bonding in GO-Ald. (Fig. 1g) [25].

#### 3.1.3. XPS analysis

XPS (X-ray photoelectron spectroscopy) analyses were performed using an XR3E2 (VG Microtech) twin anode X-ray source with Al-Kα (1486.6 eV) radiation to identify the elements in GO as well as the modified-GO. The results shown in Fig. 1-b,d,f,h were completely consistent with the results of the EDX analysis and have the expected elements for the each samples. The results confirm the successful immobilization of Ald. on GO in both covalent- (Fig. 1f) and ionic- (Fig. 1h) bonding with the presence of peaks related to the P2p and P2s binding energies at 130 eV at 170 eV, respectively.

#### 3.1.4. FTIR analysis

GO surface functionalization was studied by FTIR analysis at each step (FTIR spectroscopy RXI, Joel jsm-6360, Germany) (Fig. 2). Two absorptions at 1735 cm$^{-1}$ and 3417 cm$^{-1}$ with strong intensities represent the C=O stretching vibrations (carboxylic acid) and O-H groups on the surface of functionalized GO, respectively (Fig. 2a). A strong peak at 725 cm$^{-1}$, attributed to the stretching vibration of C-Cl, confirmed the chlorination of carboxylic acid groups in GO using SOCl$_2$. Moreover, the OH groups absorption intensity was significantly reduced at 3379 cm$^{-1}$ related to the carboxylic acid, which was another proof for the functionalization of the carboxylic groups with Cl (Fig. 2b) [25].



**Fig. 2.** FTIR spectra of (a) GO [25], (b) GO-Cl [25], (c) non-covalently- and (d) covalently modified GO by alendronate.

$$Viability(\%) = \frac{OD_{Treatedsample}}{OD_{Control}} \times 100 \qquad (4)$$

GraphPad Prism 4.7 statistical software was used in all tests to analyze significant differences in the reported data.

### 2.9. Hemolysis test

Hemolysis test was used to evaluate the nanofibers function against cell membrane disruption. Healthy volunteer blood specimens were obtained from the Bahar Afshan Research and Production Company, IRAN. For this purpose, 2 mL of blood taken from the volunteer collected

**Fig. 3.** TEM and HRTEM images of (a),(b) GO and (c),(d) GO-Ald., and (e),(f) GO*Ald. nanoparticles, respectively. The inset figures in HRTEM images represents the selected area electron diffraction (SAED) patterns obtained from the HRTEM analyses.

Immobilization of Ald. *via* the amide bonding, removes the C-Cl peak, indicating its successful immobilization on the GO surface. Also, the strong absorptions at 1056–1146 $cm^{-1}$ indicate the stretching vibrations belonging to the (P(=O)OH) group (Fig. 2c) [49]. A strong absorption at 946 $cm^{-1}$ was also assigned to the P – OH stretching vibration. Ionic immobilization of Ald. also significantly reduced the OH peak intensity (carboxylic acid), which confirms its successful immobilization. Also, the peaks related to (P(=O)OH) and P=O vibrations were quite evident in the spectrum.

*3.1.5. FE-SEM, TEM, and HRTEM analyses*

The shape and morphology of the unmodified and Ald.-modified GO NPs was studied by FESEM, TEM, and HRTEM images (Fig. 3). As shown in Fig. 3a,c,e, the GO NPs have a multi-layer sheet arrangement with wrinkled structure and have a very homogeneous morphology in agreement with the literature [25,50]. GO NPs also retained their sheet

structure after functionalization, indicating the stability of the NPs. HRTEM images were taken on a FEI Tecnai G2 F20 Super Twin TEM with a field emission gun at 200 kV. From HRTEM images, dark spots indicate Ald. immobilization on the GO surface (Fig. 3d,f). This can be proved by comparing HRTEM image of GO (Fig. 3b) with those functionalized with Ald. (Fig. 3d,f). From this viewpoint, both GO-Ald. and GO*Ald. were successfully immobilized on the GO surface.

*3.2. Studies over the characterization of nanofibrous scaffolds*

*3.2.1. FESEM, TEM, HRTEM, and fiber diameter distribution analyses*

*3.2.1.1. Gel/PCL scaffold.* Morphology of Gel/PCL-GO and Gel/PCL scaffolds were studied using a Field emission scanning electron microscopy (FE-SEM) TESCAN MIRA3 instrument (Fig. 4&5). Also, fiber diameter distribution of the nanofibers was measured by a so-called "by
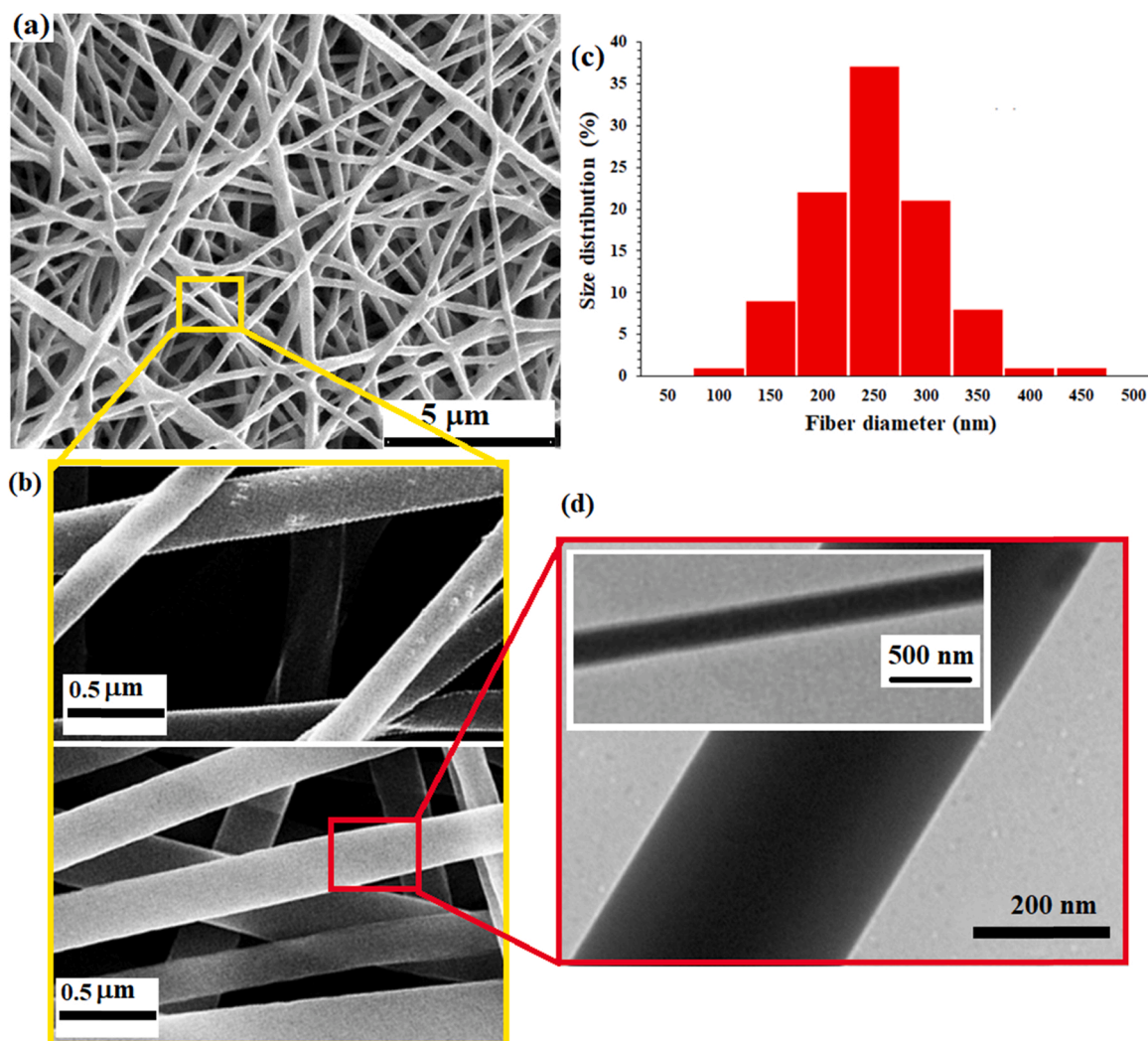
**Fig. 4.** (a), (b) FESEM images [25], (c) fiber diameter distribution [25], and (d) TEM image of Gel/PCL nanofibrous scaffold.

hand'' method [51], in which the width (W) and length (L) of each fiber was measured for 200 fibers by a numerical caliper. Based on the results, Gel/PCL and Gel/PCL-GO nanofibers had an almost narrow fiber diameter distribution with an average diameter of 250 nm (Fig. 4&5). However, the smaller diameter of the GO-containing nanofibers than Gel/PCL, demonstrates the suitable interaction of GO in the nanofiber framework. Electrical conductivity and viscosity of a solution are two important factors in electrospinning that affect the diameter of nanofibers [25,52]. Previous reports indicated that decreasing the solution viscosity and increasing of electrical conductivity, reduce the nanofibers diameter [53]. In the present study, the electrical conductivity of the solution increased after the addition of GO [54,55]. The main reason for decreasing the nanofibers diameter was the high electrical conductivity of the solution, which during the electrospinning process, leads to the stronger electrostatic repulsion forces at negative charges accumulated in the syringe [56]. The observed homogeneous morphology for the nanofibers showed the suitable interaction of Gel and PCL solution phases (as well as with GO in Gel/PCL-GO nanofibers).

Previous reports show that the electrospinning process is dependent on viscosity of the solution, and directly affects the diameter of the resulting nanofibers [57,58]. In general, during electrospinning of a polymer solution, the polymer solution jet is subjected to aerodynamic drag [59]. Shear forces in polymer solutions directly affect the fiber stretching and subsequently the fiber diameter distribution [58,59]. The higher viscosity of the polymer solution causes an irregular flow of air

exiting the nozzle and therefore requires more airflow for electrospinning, which leads to a greater distribution of nanofiber diameters (changes in airflow cause changes in the amount of stretching and shearing on the fibers) [58,60]. As the viscosity of a polymer solution increases, the fibers become more difficult and unstable to stretch, increasing the nanofiber diameter. On the other hand, the electrostatic repulsive forces responsible for controlling the formation of fibers in electrospinning overcome the surface tension, and the resulting fiber diameter is the result of these forces [58]. In this study, with increasing viscosity in PCL-GO-Ald. and PCL-GO*Ald. solutions, the diameter of the nanoparticle fiber increased slightly.

*3.2.1.2. Gel/PCL-GO scaffold.* TEM and HRTEM images also confirmed the suitable dispersion and proper interaction of GO with the nanofibrous scaffolds. As shown in Fig. 5b, GO sheets are well coated on the nanofibers, and this structure was responsible for the high mechanical strength observed for the nanofibers compared to the GO–free fibers. In addition, the HRTEM images clearly show the arrangement of the GO sheets along the Gel/PCL fibers as shown in Fig. 5b (Fig. 5d,e). Due to the interaction of GO NPs in Gel/PCL-GO, the fiber diameter distribution in this nanofiber has shifted to smaller diameters, in full agreement with the previous reports (Fig. 5f) [61,62].
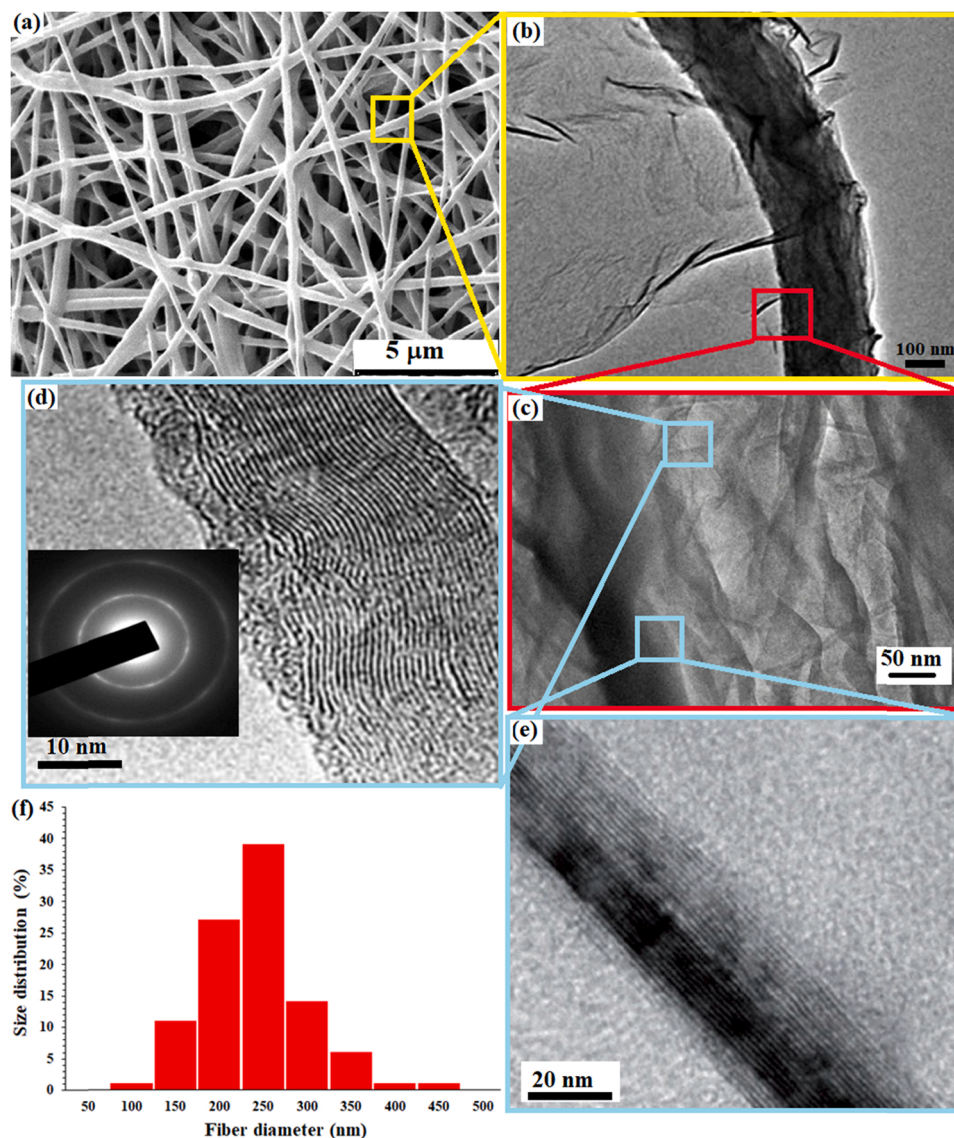
**Fig. 5.** (a) FESEM [25], (b), (c) TEM images, (c)-(e) HRTEM images, and (f) fiber diameter distribution of Gel/PCL-GO nanofibrous scaffold [25]. The inset figure (d) in HRTEM images represents the SAED pattern obtained from the HRTEM analysis.

**Table 1**
Viscosity measurement of polymeric solutions.

| Polymeric solution | PCL [25] | Gelatin [25] | PCL-GO [25] | PCL-GO-Ald. | PCL-GO*Ald. |
|---|---|---|---|---|---|
| Viscosity (cp) | 448.7 | 398.7 | 504.6 | 508.1 | 508.8 |

**Table 2**
Electrical conductivity measurement of 100 cm$^2$ of Gel/PCL [25], Gel/PCL-GO (2.5% graphene) [25], Gel/PCL-GO-Ald. (2.5%GO, 0.19 wt% Ald.), and Gel/PCL-GO*Ald. (2.5%GO, 0.25 wt% Ald.) hybrid nanofibrous scaffolds.

| Sample | Electrical conductivity (μS/cm) | Impedance (Ω) | Average thickness (nm) |
|---|---|---|---|
| Gel/PCL | 3.1 | 1995 | 250 |
| Gel/PCL-GO | 30.6 | 320 | 248 |
| Gel/PCL-GO-Ald. | 31.4 | 309 | 252 |
| Gel/PCL-GO*Ald. | 32.3 | 300 | 252 |

### 3.3. Physiochemical characterization of the nanofibers

#### 3.3.1. Viscosity measurement

The viscosity of the polymer solutions was measured using a Brookfield viscometer, DV-II+pro (USA) with a 45 rpm spindle rotation rate [63]. The results of measuring the viscosity of gelatin, PCL, and PCL-GO solutions were shown in Table 1. The increase in viscosity of the GO-containing nanofibers can be attributed to π-π stacking interactions [25,51]. In another word, loading of GO leads to the reduction in free volumes at the interface of GO nanosheets and PCL polymer chains. In fact, the presence of O and N in the GO framework provides a hydrogen bond between Ald. and PCL chains and increases their interactions, and consequently increases the solution viscosity in the GO-containing nanofibers [25,39,52]. Immobilization of Ald. on GO did not have a significant effect on the resulting polymer mixture viscosity and the slight increase observed in viscosity can be attributed to the increase in hydrogen bond interactions between the GO plates modified with Ald. and PCL. As shown in Table 1, PCL-GO-Ald. and PCL-GO*Ald. have the similar viscosity equal to 508.1 cp and 508.8 cp, respectively.

**a) Covalent bonding**



**b) Non-covalent (ionic) bonding**
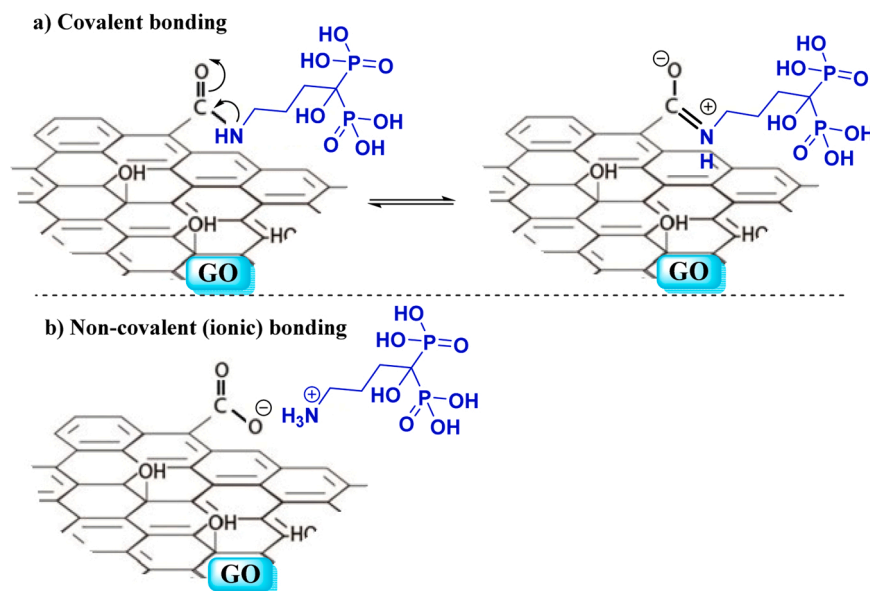


**Scheme 2.** The plausible interaction of Ald. with GO *via* (a) amide bond resonance and (b) ionic interaction.

**Table 3**
Mechanical properties of Gel/PCL [25], Gel/PCL-GO [25], Gel/PCL-GO*Ald., and Gel/PCL-GO-Ald. scaffolds.

| Nanofiber | Stress at break (MPa) | Strain at break (%) | Ultimate tensile strength (MPa) |
|---|---|---|---|
| Gel/PCL | $3.5 \pm 0.1$ | $116 \pm 6.2$ | $8.5 \pm 0.3$ |
| Gel/PCL-GO | $5.2 \pm 0.2$ | $93 \pm 7.1$ | $14.4 \pm 0.3$ |
| Gel/PCL-GO*Ald. | $5.4 \pm 0.2$ | $93 \pm 5.7$ | $14.7 \pm 0.4$ |
| Gel/PCL-GO-Ald. | $5.3 \pm 0.2$ | $93 \pm 3.1$ | $15.1 \pm 0.3$ |

**Table 4**
Swelling measurements of Gel/PCL [25], Gel/PCL-GO [25], Gel/PCL-GO-Ald., and Gel/PCL-GO*Ald. nanofibers after 5 h.

| Solvent | Swelling of nanofiber (mL/g) | | | |
|---|---|---|---|---|
| | Gel/PCL | Gel/PCL-GO | Gel/PCL-GO-Ald. | Gel/PCL-GO*Ald. |
| PBS buffer | 14.0 | 18.5 | 18.4 | 17.8 |

### 3.3.2. Electrical conductivity measurements

Table 2 shows the results of the electrical conductivity measurements on 100 cm$^2$ area of Gel/PCL, Gel/PCL-GO (2.5% GO), Gel/PCL-GO-Ald. (2.5%GO, 0.19 wt% Ald.), and Gel/PCL-GO*Ald. (2.5%GO, 0.25 wt%

Ald.) hybrid nanofibrous scaffolds. The results indicated a significant decrease in the impedance of the nanofibers after the addition of GO (Increase of the electrical conductivity of the nanofiber scaffolds) (Table 2). According to the results, the incorporation of GO NPs into the electrospun nanofibers framework leads to a significant increase in the electrical conductivity of the scaffolds from 3.1 μS/cm to 30 μS/cm for Gel/PCL and the GO-containing fibers, respectively [25]. As shown in Fig. 5f, the fiber diameter distribution in Gel/PCL-GO has shifted slightly towards smaller diameters. In accordance with the previous reports [27,
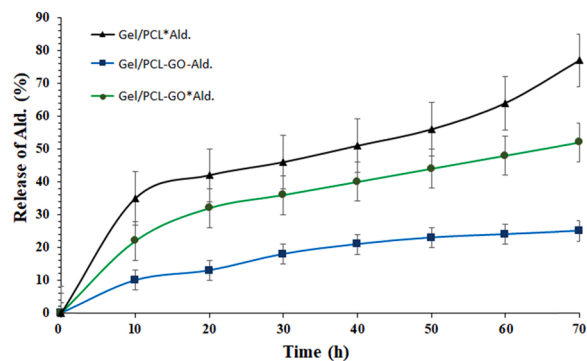


**Fig. 7.** Monitoring of release of alendronate from Gel/PCL-GO-Ald. and Gel/PCL-GO*Ald. during 70 h.
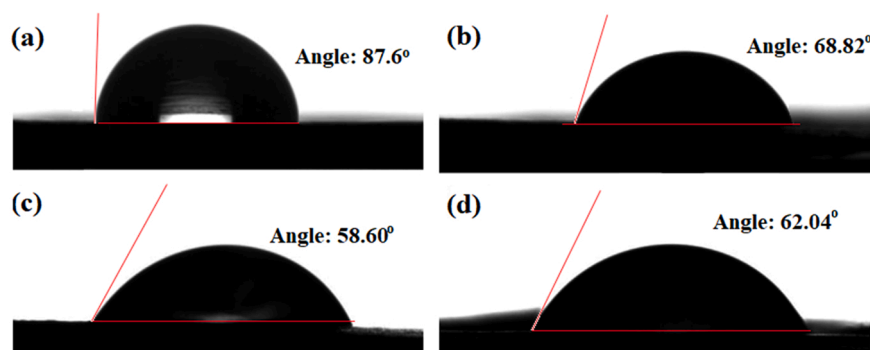


**Fig. 6.** Contact angles of the nanofiber scaffolds in pure water: (a) Gel/PCL [25], (b) Gel/PCL-GO [25], (c) Gel/PCL-GO-Ald., and (d) Gel/PCL-GO*Ald. after 3 s.
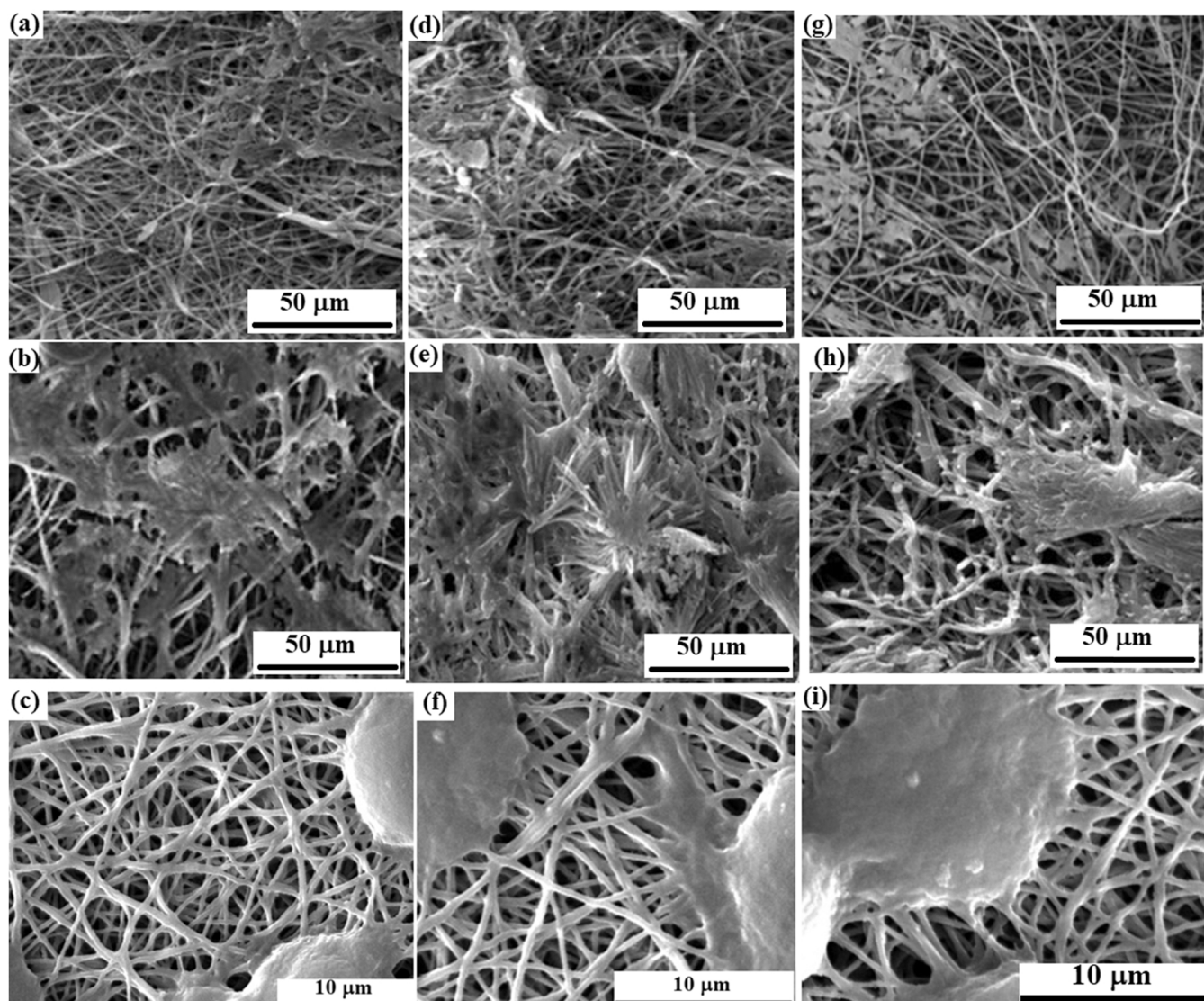
**Fig. 8.** The morphology of bone cells on the scaffolds: (a)-(c) Gel/PCL, (b)-(f) Gel /PCL-GO-Ald., and Gel /PCL-GO*Ald.

64], the addition of GO to the electrospinning solution reduces the diameter of the fibers, which results in an increase in electrical conductivity. The results indicated that the Gel/PCL nanofibers containing 2.5 wt% GO has about 11 times the electrical conductivity compared to the GO-free nanofibers. This increase in electrical conductivity was consistent with the application of scaffolds in bone tissue engineering.

The results showed that the immobilization of Ald. led to slight increase in the electrical conductivity of the nanofibers. The resulting amide bond in Gel/PCL-GO-Ald. scaffold reduces the resonance of the carbonyl groups with the aromatic rings in GO, and therefore these electrons are more involved in conductivity (Scheme 2). In the ionic (non-covalent) state, a similar explanation can be given in which the carboxylic groups become ionic by interaction with Ald. and its resonance with the GO-aromatic rings is reduced and thus the electrical conductivity of the scaffold increases (Scheme 2). Comparison of the electrical conductivity of GO with rGO (with much fewer carboxylic groups than GO), also confirms the explanation, that the reduction of carboxylic acid groups significantly increases the electrical conductivity in rGO [61,62]. These two interactions were shown in Scheme 2.

Differences in how Ald. immobilized on GO, also affected the electrical conductivity of the resulting fibers. As shown in Table 2, Gel/PCL-GO*Ald. (with ionic/H-bonding immobilization of Ald. on GO) provides higher electrical conductivity than Gel/PCL-GO-Ald. (with a covalent amide bond). This difference can be attributed to a weaker bond/interaction than a covalent amide bond, that leads to a stronger electron current for GO.

### 3.3.3. Mechanical properties

The properties of nanofibers, their geometric arrangement and entanglement between the fibers, determine the properties of the prepared nanofibers, that were studied by tensile-strain test in this wok. Table 3 shows the tensile measurement for each Gel/PCL, Gel/PCL-GO, Gel/PCL-GO*Ald., and Gel/PCL-GO-Ald. nanofibers. According to the previous reports [25,65], GO significantly enhances the mechanical properties of nanofibers in comparison with Gel/PCL fiber, that was also shown in this study (Table 3). This increase is the result of strong interaction of GO with Gel and PCL fibers. Various studies have shown that the addition of more than 0.1 wt% of GO to the nanocomposite reduces the Young's modulus as well as the tensile strain [25,66], but in this study it was shown that at 2.5 wt% of GO, Gel/PCL-GO nanofiber has superior mechanical properties than Gel/PCL nanofiber, which can be attributed to the proper distribution and strong interaction between polymer chains and GO. Proper distribution of GO NPs in the scaffold nanofibers (Fig. 5) was responsible for the high mechanical strength observed for the GO-containing scaffolds. The strain at break was also reduced after the addition of GO, which indicates an improvement in the
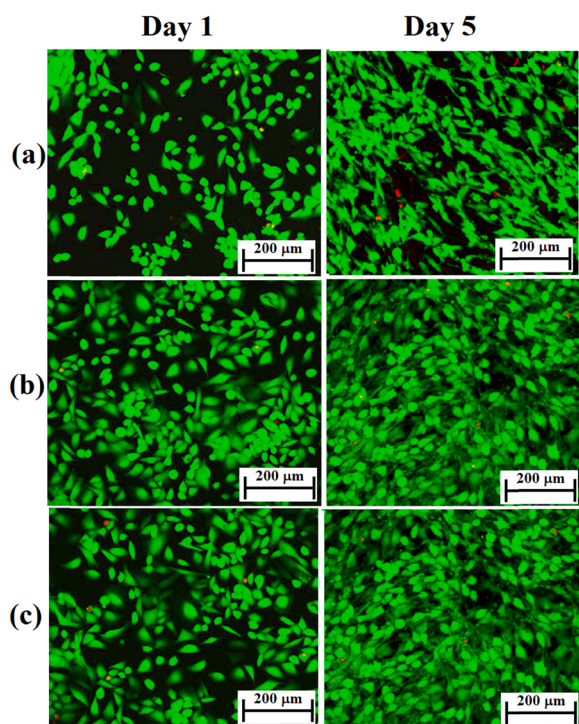
**Fig. 9.** Fluorescence microscopy images of G-292 cells on (a) Gel/PCL, (b) Gel/PCL-GO-Ald., and (c) Gel/PCL-GO*Ald. after 1 and 5 days of cell culture.

mechanical properties and stiffness of the nanofibers (Table 3). Immobilization of Ald. had no significant effect on the mechanical properties of the fibers. As shown in Table 3, the tensile strength for Gel/PCL-GO*Ald. and Gel/PCL-GO-Ald. nanofibers was about 15 MPa.

### 3.3.4. Swelling measurements

Swellability studies on the nanofibers showed that hydrophilicity on nanofibers has increased (Table 4). 14.0 mL/g swelling was measured for Gel/PCL nanofiber scaffold, which increased to 18.5 mL/g in Gel/PCL-GO scaffold. Due to the high aspect ratio associated with GO NPs, they provide high water adsorption capacity for the GO-containing scaffolds [25]. Ald. immobilization had no significant effect on swellability of the scaffolds and remained constant after Ald. immobilization.

### 3.3.5. Investigation of contact angle of the nanofiber scaffolds to evaluate the amount of hydrophilicity

The hydrophobic-hydrophilicity properties of the scaffolds were determined by measuring the contact angle of a water molecule on the scaffolds using a Sony Color Video Camera, SSC-DC318P model. For this goal, 1 μL of distilled water was placed on the nanofiber surface with a syringe and after 3 s of placement, a photo was taken. Contact angle was reported using "Image J" software. The tendency of nanofibers to absorb or repel water greatly affects their application in tissue engineering. Generally, nanofibers with hydrophilic nature increase adhesion and subsequent cell proliferation in comparison with nanofibers with hydrophobic nature with insufficient surface sites to interact with cells. Hydrophilicity also improves the distribution of cells throughout the scaffold surface and leads to the suitable supplementation of oxygen and other nutrients to the scaffold. The contact angle of water droplets with the scaffold was the exact measure of hydrophobicity or hydrophilicity of a scaffold. Fig. 6 shows the results of contact angle measurements for Gel/PCL, Gel/PCL-GO, Gel/PCL-GO-Ald., and Gel/PCL-GO*Ald. nanofibers. Hydrophobic nature of PCL with a contact angle of about 145 ± 1° [8,25,52], has largely limited its application in tissue engineering. On the other hand, Gel, is a hydrophilic polymer, and its combination with PCL greatly increases the hydrophilicity of the resulting Gel-PCL

nanofiber scaffolds. This difference was reflected in the contact angles of Gel/PCL and PCL scaffolds. The results indicate that the addition of GO to Gel/PCL nanofibers increases the hydrophilicity of scaffolds [25]. This increase can be attributed to the presence of hydrophilic functional groups that resulted in a hydrogen bond between Gel and PCL polymer. As showed in Fig. 6b, after the addition of GO NPs to PCL fibers, the contact angle in Gel/PCL-GO deceased to 68.83° (Fig. 6b) [25]. In this viewpoint, the electrospun nanofiber scaffolds are a suitable candidate for application in biomedical applications for sake of their increased hydrophilicity. The minimum contact angle value was 58.60° for Gel/PCL-GO-Ald. (Fig. 6c). This decrease was due to the immobilization of Ald. groups on the GO surface that has the ability to create a strong hydrogen bond with water. The contact angle for the immobilized Ald. *via* ionic interactions increased slightly (Fig. 6d).

### 3.4. Release studies of alendronate from the nanofibrous scaffolds

Alendronate release from Gel/PCL-GO-Ald., Gel/PCL-GO*Ald. and Gel/PCL*Ald. nanofibers was investigated at 37 °C in phosphate buffer (Fig. 7). The effect of the presence of GO on the structure of the fibers in the study of Ald. release showed that in the absence of GO, in the first 10 h, the sudden release of the drug occurs by 35%, and reaches 77% for 70 h. The results showed that alendronate release rate at 37 °C in the first 10 h was about 22% for Gel/PCL-GO*Ald. nanofibers. Whereas, for Gel/PCL-GO-Ald. only 10% Ald. release was observed in the same time period. This release was slow and controlled due to covalent immobilization of Ald. (*via* strong amide bond) on GO, which occurs due to slow hydrolysis in the buffer medium. The sudden release of the drug in the first 10 h can be attributed to the presence of Ald. with ionic and cleavable hydrogen bonded to the nanofiber scaffolds. Also, the drug release curves from Gel/PCL-GO-Ald. and Gel/PCL-GO*Ald. nanofibers show that the release rate for Gel/PCL-GO-Ald. has decreased over time. Release values after 70 h were measured for Gel/PCL-GO-Ald. and Gel/PCL-GO*Ald. as 25% and 52% of the total amount of Ald. loaded on GO, respectively. From Fig. 7, it can be seen that with the addition of GO, the release was slower, which can be attributed to the special ability of GO to form ionic (hydrogen) or covalent bonds with drug molecules.

Given that the amide bond is a strong covalent bond and is not easily hydrolyzed at pH 7, two possible reasons can be given for it: (1) distortion at the amide bond resonance and lose of double bond character that facilitates nucleophilic and (or electrophilic) attack and subsequent hydrolysis of the amide bond. On the other hand, the carbonyl group also has resonance with benzene rings in GO, which weakens the amide bond character (reduces resonance with amide bond).

(2) The proximity of Ald. immobilized on the GO surface, also deviates the amide bonds from the planar structure and allows free rotation around the C(O)-N bond. Nevertheless, Ald. release was done with a very gentle slope, that was very convenient for such a toxic drug with high side effects.

Mahesh et al. reviewed the amide bond activation in biomolecules and showed that there are various enzymes-catalyzed pathways for the cleavage of inactivated and highly stable amide bonds in body [67].

### 3.5. Investigation of cell culture on the nanofiber scaffolds

#### 3.5.1. FESEM studies

Investigation of cell growth process on biological scaffolds that mimic the extracellular matrix (ECM) is of great importance, because the prepared scaffolds must have appropriate cellular behavior. At first, the cells were spherical, and expanded with the growth process. The larger the number of flattened cells than spherical ones, represents that the scaffold is more suitable for biological applications [68,69]. In this study, G-292 cells were used to evaluate cell attachment and adhesion to the scaffolds. The morphology of osteosarcoma cells on Gel/PCL and Gel/PCL-GO-Ald. fibrous specimens after 5 days was shown in Fig. 8. The images confirm the morphology and interaction between cells and
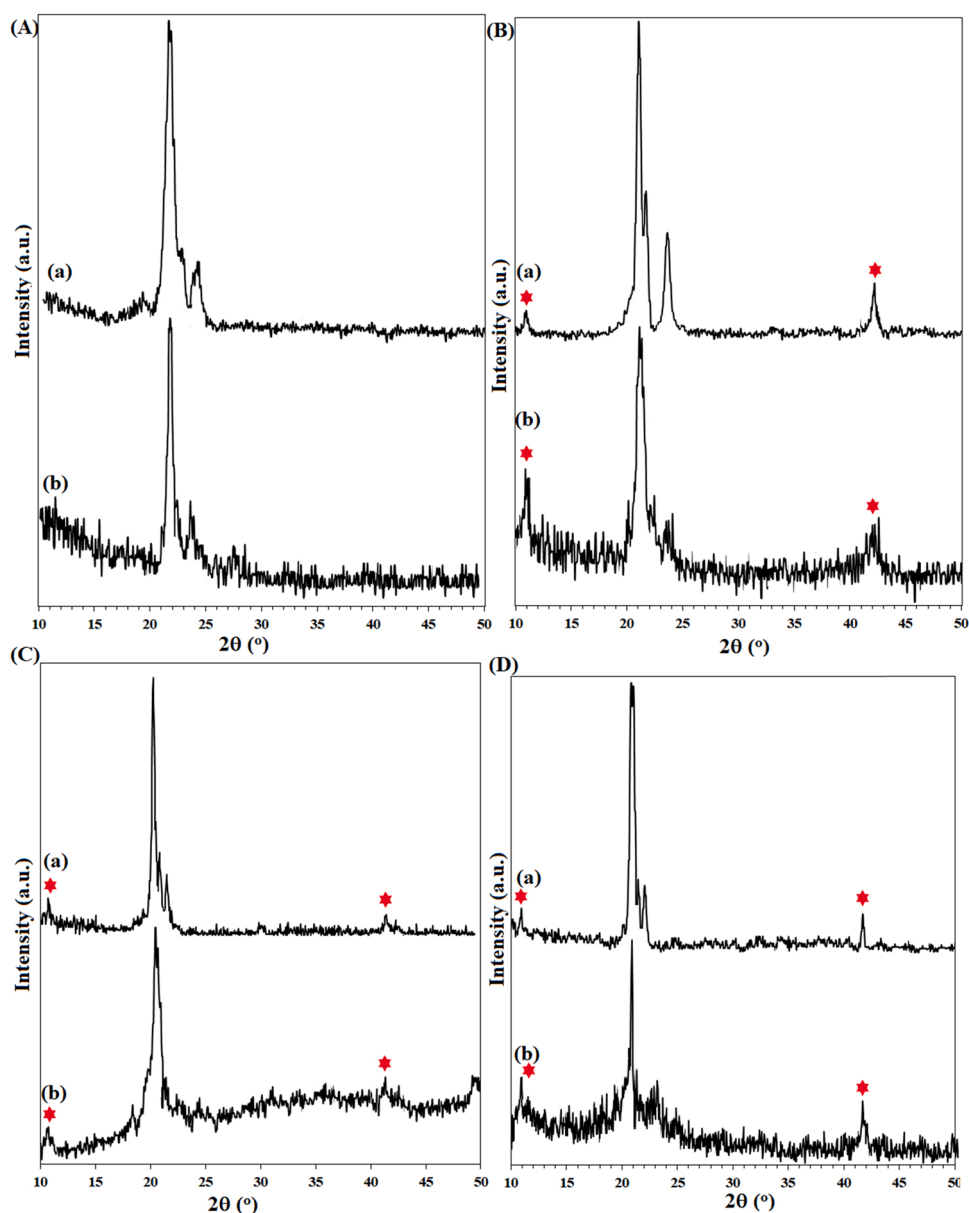
**Fig. 10.** XRD patterns of (A) Gel/PCL, (B) Gel/PCL-GO, (C) Gel/PCL-GO-Ald., and (D) Gel/PCL-GO*Ald. nanofibrous scaffolds, (a) before and (b) after 5 days of G-292 cells culture.

the nanofiber scaffolds. In this figure, a large number of cells with homogenous morphology on Gel/PCL and Gel / PCL-GO-Ald. scaffolds made good interactions in different directions of the fiber arrangement. Also, the cells retained their natural morphology and showed an interconnected cell layer on the nanofiber scaffolds.

### 3.5.2. Fluorescence technique

Cell culture on the scaffolds was also studied by fluorescence technique on a confocal fluorescence microscope (Leica Microsystem, Mannheim, Germany). As shown in Fig. 9, very few cells die within 5 days, and cell culture from day 1 to day 5 clearly reflected the biocompatibility of the scaffolds. Also, compared to Gel/PCL scaffold (Fig. 9a), cell growth on the Gel/PCL-GO scaffold was much higher in 5 days, which indicates the effect of Ald. immobilization on the biocompatibility of the resulting scaffolds and consequently the cell proliferation (Fig. 9b,c).

### 3.5.3. XRD patterns of the scaffolds before and after cell culture

XRD patterns for all of the prepared scaffolds including Gel/PCL, Gel/PCL-GO, Gel/PCL-GO-Ald., and Gel/PCL-GO*Ald. were also studied before and after cell culture. To investigate the scaffolds by XRD analysis after G-292 cell culture, immediately after cell culture on the scaffolds after 5 days of incubation, the crystalline nature of the nanofibrous scaffolds was studied on a Bruker D8/Advance powder X-ray diffractometer with Cu-Kα radiation ($\lambda = 1.54$ Å) at scanning rate of 1 step per second and $0.15°$/step. The XRD instrument was equipped with an FTS XR AirJet Sample Cooler (model XR 401, SP Industries, Inc., USA) to maintain the analysis temperature at $37.5 \pm 0.2$ °C. Fig. 10 shows the crystal structure of the scaffolds before and after cell culture. The XRD pattern of Gel/PCL scaffold shows three characteristic peaks at $2\theta = 21.5°$, $22°$, and $23.7°$ according to the crystal structure of PCL (Fig. 10A-a) [70]. Deviation of the peaks from the completely crystalline state (as sharp peaks) in pure PCL indicates the suitable blending and consequently proper interaction between PCL and amorphous Gel polymers [71]. The presence of GO NPs in Gel/PCL-GO scaffold was

**Table 5**

Antibacterial activity of Gel/PCL, Gel/PCL-GO, Gel/PCL-GO-Ald., Gel/PCL-GO*Ald. nanofiber scaffolds against *E. coli* and *S. aureus*a.

| Microorganism | Nanofiber | Growth inhibition zone (mm), Mean±SD |
|---|---|---|
| *E.coli* | Gel/PCL[25] | – |
| | Gel/PCL-GO[25] | 7 ± 0.25 |
| | Gel/PCL*Ald. (0.25 wt% Ald.) | 15 ± 0.26 |
| | Gel/PCL-GO-Ald. (2.5%GO, 0.19 wt% Ald.) | 15 ± 0.14 |
| | Gel/PCL-GO*Ald. (2.5%GO, 0.25 wt% Ald.) | 19 ± 0.55 |
| | Tetracycline (30 μg)[25] | 21 ± 0.00 |
| *S. aureus* | Gel/PCL[25] | – |
| | Gel/PCL-GO[25] | 9 ± 0.25 |
| | Gel/PCL*Ald. (0.25 wt% Ald.) | 16 ± 0.22 |
| | Gel/PCL-GO-Ald. (2.5%GO, 0.19 wt% Ald.) | 16 ± 0.10 |
| | Gel/PCL-GO*Ald. (2.5%GO, 0.25 wt% Ald.) | 22 ± 0.42 |
| | Tetracycline (30 μg)[25] | 24 ± 0.00 |

a The disk diffusion test was repeated triple for each nanofiber and a mean zone diameter was reported.

confirmed by the appearance of a low-intensity peak at $2\theta = 11°$ (The peaks related to the GO crystal structure were indicated with an asterisk in the X-ray diffraction patterns) (Fig. 10B-a) [72]. The lack of significant change in the XRD patterns of Gel/PCL-GO and Ald.-containing scaffolds indicates the proper dispersion of GO NPs as well as Ald. in the scaffolds (Fig. 10B-a, C-a, D-a).

Cell culture on the scaffolds caused the peaks to deviate from the crystalline state, which was more for the scaffolds containing Ald. In addition, due to the biodegradable nature of Gel/PCL scaffolds in the physiological environment [4–6], the scaffolds undergo some degradation, which causes the peaks to deviate from the crystalline state. In accordance with the results of MTT analysis (Section 3.7), these scaffolds have higher biological properties and less toxicity than other. No change in the crystal structure of the scaffolds after cell culture indicates the preservation of the crystal structure of the scaffolds. As shown in Fig. 10, the largest deviations from the crystalline state were related to the Ald.-containing scaffolds, so that in accordance with the FESEM images, the highest amount of cell culture has been done on them. Also in agreement with the MTT results (presented in Section 3.7), Ald.-containing scaffolds have higher biocompatibility than Gel/PCL and Gel/PCL-GO scaffolds. In general, cell culture was performed successfully on all studied scaffolds and little cell death was observed.

### 3.5.4. The relationship between electrical conductivity and cell culture on nanofibrous scaffolds

The history of the discovery of the electrical properties of bone tissue dates back to the 1950 s. This suggests that bone tissue responds to external pressures by having an internal electrical field, changes the way bone cells proliferate [73]. Previous reports have shown that external electrical induction can also increase the growth, proliferation, and differentiation of osteoblasts and stem cells, which ultimately improves the speed of bone repair [25,74]. Shao et al. has been reported the use of electrically conductive polylactic acid nanofibers in combination with multi-walled carbon nanotubes (PLA/MWCNTs) to improve the bone cell function [75]. In another study, Guex et al. [76] developed scaffolds of poly(3,4-ethylenedioxythiophene) polystyrene sulfonate (PEDOT: PSS) to enhance bone cell proliferation with electrical conductivity of 140 μS/cm, which after 28 days in culture medium, decreased to 6.1 μS/cm. This reduction in conductivity can be attributed to the initial burst release of secondary dopant 4-dodecylbenzenesulfonic acid (DBSA) [72]. The results of cellular tests indicated a positive effect of these electrically conductive scaffolds on improving bone cell function. In the present study, the positive effect of the electrical conductivity of the Gel/PCL-GO-Ald. and Gel/PCL-GO*Ald. scaffolds on osteogenic cells was confirmed.

### 3.6. Antibacterial activity

Antibacterial activity of Gel / PCL, Gel / PCL-GO, Gel / PCL-GO-Ald., and Gel / PCL-GO*Ald. scaffolds against *Staphylococcus aureus* and *E. coli* bacteria strains was investigated using the disk diffusion assay (Table 5). No antibacterial activity was found for Gel/PCL nanofiber against both bacteria. Gel/PCL-GO scaffold showed moderate inhibition in agreement with the literature [77–79]. Conversely, in the two scaffolds containing Ald. (Covalently and ionically immobilized), the growth inhibition zone was observed in the range of 15–22 mm (Table 5). The remarkable point was the higher effectiveness of Gel/PCL-GO*Ald. than Gel/PCL-GO-Ald., which can be directly attributed to the ionic/H-bonding immobilization of Ald. on GO. It seems that the antibacterial effect on the scaffolds was applied by a mechanism that depends on the release of the drug from the GO surface; according to the previous results, Ald. was more easily released from the Gel/PCL-GO*Ald. scaffold (immobilization of Ald. *via* ionic/H-bonding), than when immobilized by a covalent bonding on GO (Fig. 7). Also, Gel / PCL-GO-Ald. and Gel/PCL-GO*Ald. scaffolds were more effective against *S. aureus* than *E. Coli,* in agreement with the previously published articles [45,46]. As shown in Table 5, scaffolds containing Ald.
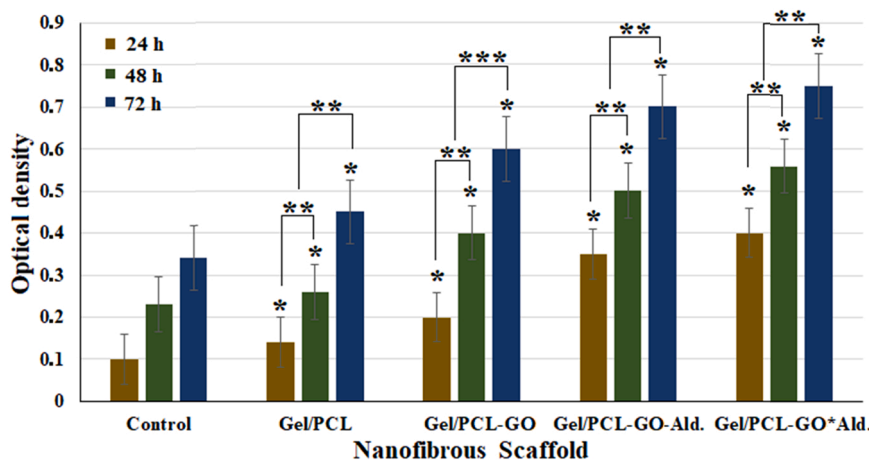


**Fig. 11.** MTT assay of different nanofibrous scaffolds including a control sample, Gel/PCL [25], Gel/PCL-GO [25], Gel/PCL-GO-Ald., and Gel/PCL-GO*Ald. after 1, 2 and 3 days. Error bars represent means ± SD for n = 3. cell viability of all samples was significant compared with the control, * $P < 0.05$, * * $P < 0.01$, * * * $P < 0.001$.
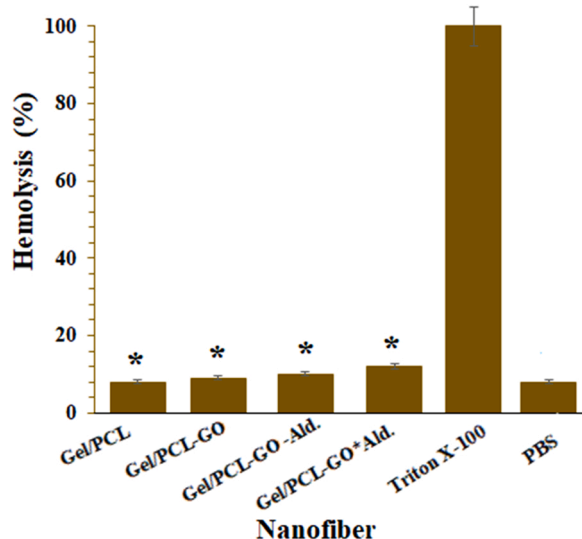
**Fig. 12.** Hemolysis test over the prepared nanofibers. Values represent the mean ± SD, n = 3, * $p < 0.0001$ corresponding with positive control group (Triton X-100).

have the same antibacterial properties as tetracycline, which was acceptable for very small amounts of immobilized Ald. on the scaffolds. The results showed that the Gel/PCL-GO-Ald. and Gel / PCL-GO*Ald. scaffolds were able to inhibit bacterial growth simultaneously with cell viability. The antibacterial activity of Gel/PCL*Ald. scaffold against *E. coli* and *E. aureus* was measured at 15 and 16 mm, respectively. According to the Ald. release results from the Gel/PCL*Ald. scaffold (for 24 h, that was the period time of the disk diffusion analysis), the difference between Ald. release from Gel/PCL*Ald. and Gel/PCL-GO*Ald. scaffold was only 10%, while the antibacterial activity of Gel/P-CL*Ald. scaffold was approximately equal to that of Gel/PCL-GO-Ald. scaffold with the release of about 14% for 24 h. This difference can be directly attributed to the antibacterial effect of GO as well as its synergistic effect due to its interaction with Ald. in the scaffolds; because by comparing the antibacterial activity of Gel/PCL and Gel/PCL-GO scaffolds, it can be concluded that the antibacterial activity in these scaffolds was related to the presence of GO. On the other hand, the results showed that Gel/PCL scaffolds have low mechanical strength and electrical conductivity than their GO-based nanocomposites in accordance with the previous reports [27,28,65]. Also the lack of loading and interaction of drug molecules with these scaffolds causes the huge release of the drug in the medium (Fig. 7), so it was not suitable for drugs with adverse side effects. In addition, the presence of GO increases the hydrophilicity of Gel/PCL scaffold (Table 4 & Fig. 6), a parameter that is very important for scaffolds used in tissue engineering. The high surface-to-volume ratio of NPs has led to its use as a reliable filler for drug loading and the addition of desired properties to a fiber, such as mechanical strength, for use in bone tissue engineering.

### 3.7. Evaluation of toxicity and biocompatibility of the nanofibrous scaffolds (MTT assay)

MTT test is a colorimetric method based on the formation of insoluble purple formazan crystals due to the reduction and breakdown of yellow MTT crystals by the succinate dehydrogenase enzyme. The amount and intensity of dye produced in this test is directly related to the number of cells that are metabolically active. Fig. 11 shows the MTT test results of these cells after 1, 2 and 3 days on Gel/PCL, Gel/PCL-GO, Gel/PCL-GO-Ald., and Gel/PCL-GO*Ald. scaffolds and also a control sample (absence of any scaffolds). As shown in the figure, on the first day, the rate of cell viability in Gel/PCL-GO-Ald. and Gel/PCL-GO*Ald.

was significantly different from other groups, which was much higher on the second and third days. As shown in Fig. 11, cell viability percentage on Gel/PCL-GO-Ald. and Gel/PCL-GO*Ald. was also greater than the control. However, with increasing incubation time (days 1, 2, and 3), the cell viability percentage increased, which was much higher for the alendronate-containing nanofibers and on the third day of incubation, the number of living cells on the alendronate-containing fibrous scaffolds has been maximized. Considering the values shown in the figure, more viable cells were seen on the fibrous scaffolds than in the control sample. Therefore, based on the results, it can be concluded that the GO-containing fiber scaffolds have no toxicity, and their biocompatibility was suitable for use in bone tissue engineering applications, in agreement with the literature [17,80]. More and significant cell viability percentage for GO-containing nanofibers can be attributed to the increased hydrophilicity and greater protein uptake by the fibers that led to the excellent biological properties of GO within the nanofiber structures [81,82]. In addition, the presence of immobilized Ald. on GO, has significantly increased its biocompatibility, which also indicated a reduction in the toxicity of GO.

### 3.8. Hemolysis test

Fig. 12 shows the results of the study of the effect of different nanofiber scaffolds on hematopoiesis (hemolysis test at physiological pH). As shown in the figure, all scaffolds had acceptable hematopoiesis and do not exceed 12% and were similar to PBS effect. Even in Ald.-containing fibers, no lysis of red blood cells was observed after centrifugation. The maximum lysis was observed for Gel/PCL-GO*Ald. equal to 12%. The results indicated that the loading of Ald. has the minimal toxicity on the nanofibers and provides their possible application in bone tissue engineering with more confidence.

### 4. Conclusion

In this work, Gel/PCL nanofibers reinforced by GO@alendronate was prepared as a promising, safe, and biocompatible nanofiber with high antibacterial activity for the possible use in bone tissue engineering. Alendronate as a bisphosphonate drug was immobilized on GO *via* covalent as well as ionic/H-bonding. The addition of gelatin as well as GO gave high hydrophilic properties to the resulting nanofibers, that was a vital factor for the application in bone tissue engineering. The MTT assay revealed that the presence of immobilized Ald. on GO significantly increased its biocompatibility, which also indicates a decrease in the toxicity of GO. Also, the hemolysis test confirmed that the loading of Ald. has the least toxicity on the fibers, making their application in bone tissue engineering with more confidence. The results showed that Gel/PCL-GO-Ald. and Gel/PCL-GO*Ald. scaffolds were able to inhibit bacterial growth simultaneously with cell viability. The scaffolds suggested a possible drug delivery system with a controlled release of Ald., as a high side effects-containing drug, from the scaffolds surface.

**CRediT authorship contribution statement**

**Hendrik Setia Budi:** Software, Data curation, Visualization, Writing – review & editing. **Alla Davidyants:** Data curation, Formal analysis, Investigation, Methodology, Writing – review & editing. **Mohammad Rudiansyah:** Project administration, Supervision, Validation, Roles/Writing – original draft, Writing – review & editing. **Mohammad Javed Ansari:** Data curation, Validation, Visualization, Writing – review & editing. **Wanich Suksatan:** Software; Data curation, Visualization, Writing – review & editing. **Mohammed Q. Sultan:** Software, Data curation, Visualization, Writing – review & editing. **Abduladheem Turki Jalil:** Software, Formal analysis; Methodology. **Milad Kazemnejadi:** Project administration, Supervision, Validation, Roles/Writing – original draft, Writing – review & editing.

## Declaration of Competing Interest

The authors declare that they have no conflict of interest.

## Data Availability

No data was used for the research described in the article.

## Acknowledgements

## Appendix A. Supporting information

Supplementary data associated with this article can be found in the online version at doi:10.1016/j.mtcomm.2022.104108.

## References

[1] D.K. Patel, S.D. Dutta, J. Hexiu, K. Ganguly, K.T. Lim, Bioactive electrospun nanocomposite scaffolds of poly (lactic acid)/cellulose nanocrystals for bone tissue engineering, Int. J. Biol. Macromol. 162 (2020) 1429–1441.

[2] S. Gautam, C. Sharma, S.D. Purohit, H. Singh, A.K. Dinda, P.D. Potdar, C.F. Chou, N.C. Mishra, Gelatin-polycaprolactone-nanohydroxyapatite electrospun nanocomposite scaffold for bone tissue engineering, Mater. Sci. Eng. C 119 (2021), 111588.

[3] W. Lin, M. Chen, T. Qu, J. Li, Y. Man, Three-dimensional electrospun nanofibrous scaffolds for bone tissue engineering, J. Biomed. Mater. Res. Part B 108 (2020) 1311–1321.

[4] B. Maharjan, V.K. Kaliannagounder, S.R. Jang, G.P. Awasthi, D.P. Bhattarai, G. Choukrani, C.H. Park, C.S. Kim, *In-situ* polymerized polypyrrole nanoparticles immobilized poly (ε-caprolactone) electrospun conductive scaffolds for bone tissue engineering, Mater. Sci. Eng. C 114 (2020), 111056.

[5] W.W. Khodir, V. Guarino, M.A. Alvarez-Perez, C. Cafiero, L. Ambrosio, Trapping tetracycline-loaded nanoparticles into polycaprolactone fiber networks for periodontal regeneration therapy, J. Bioact. Compat. Polym. 28 (2013) 258–273.

[6] H.W. Kim, J.C. Knowles, H.E. Kim, Hydroxyapatite/poly (ε-caprolactone) composite coatings on hydroxyapatite porous bone scaffold for drug delivery, Biomaterials 25 (2004) 1279–1287.

[7] B. Bochicchio, K. Barbaro, A. De Bonis, J.V. Rau, A. Pepe, Electrospun poly (d, l-lactide)/gelatin/glass-ceramics tricomponent nanofibrous scaffold for bone tissue engineering, J. Biomed. Mater. Res. Part A 108 (2020) 1064–1076.

[8] S. Tarafder, S. Bose, Polycaprolactone-coated 3D printed tricalcium phosphate scaffolds for bone tissue engineering: in vitro alendronate release behavior and local delivery effect on in vivo osteogenesis, ACS Appl. Mater. Interfaces 6 (2014) 9955–9965.

[9] X. Ma, Z. He, F. Han, Z. Zhong, L. Chen, B. Li, Preparation of collagen/hydroxyapatite/alendronate hybrid hydrogels as potential scaffolds for bone regeneration, Coll. Surf. B 143 (2016) 81–87.

[10] F. Von Knoch, C. Jaquiery, M. Kowalsky, S. Schaeren, C. Alabre, I. Martin, H. E. Rubash, A.S. Shanbhag, Effects of bisphosphonates on proliferation and osteoblast differentiation of human bone marrow stromal cells, Biomaterials 26 (2005) 6941–6949.

[11] G. Duque, D. Rivas, Alendronate has an anabolic effect on bone through the differentiation of mesenchymal stem cells, J. Bone Miner. Res. 22 (2007) 1603–1611.

[12] G.-I. Im, S.A. Qureshi, J. Kenney, H.E. Rubash, A.S. Shanbhag, Osteoblast proliferation and maturation by bisphosphonates, Biomaterials 25 (2004) 4105–4115.

[13] J.S. Chen, P.N. Sambrook, Antiresorptive therapies for osteoporosis: a clinical overview, Nat. Rev. Endocrinol. 2 (2012) 81–91.

[14] P.J.J. Prinsloo, D.J. Hosking, Alendronate sodium in the management of osteoporosis, Ther. Clin. Risk Manag. 2 (2006) 235–249.

[15] W. Shi, X. Zhang, L. Bian, Y. Dai, Z. Wang, Y. Zhou, S. Yu, Z. Zhang, P. Zhao, H. Tang, Q. Wang, Alendronate crosslinked chitosan/polycaprolactone scaffold for bone defects repairing, Int. J. Biol. Macromol. 204 (2022) 441–456.

[16] H. Toker, H. Ozdemir, H. Ozer, K. Eren, A comparative evaluation of the systemic and local alendronate treatment in synthetic bone graft: a histologic and histomorphometric study in a rat calvarial defect model, Oral. Surg. Oral. Med. Oral. Pathol. Oral. Radiol. 114 (2012) S146–S152.

[17] Ł. Rumian, C. Wolf-Brandstetter, S. Rößler, K. Reczyńska, H. Tiainen, H.J. Haugen, D. Scharnweber, E. Pamuła, Sodium alendronate loaded poly (l-lactide-co-glycolide) microparticles immobilized on ceramic scaffolds for local treatment of bone defects, Regen. Biomater. (8) (2020) rbaa012.

[18] J.E.N. Dolatabadi, H. Hamishehkar, M. Eskandani, H. Valizadeh, Formulation, characterization and cytotoxicity studies of alendronate sodium-loaded solid lipid nanoparticles, Coll. Surf. B 117 (2014) 21–28.

[19] N.Z. Laird, T.M. Acri, J.L. Chakka, J.C. Quarterman, W.I. Malkawi, S. Elangovan, A. K. Salem, Applications of nanotechnology in 3D printed tissue engineering scaffolds, Eur. J. Pharm. Biopharm. 161 (2021) 15–28.

[20] M. Kazemnejadi, B. Mahmoudi, Z. Sharafi, M.A. Nasseri, A. Allahresani, M. Esmaeilpour, Synthesis and characterization of a new poly α-amino acid Co(II)-complex supported on magnetite graphene oxide as an efficient heterogeneous magnetically recyclable catalyst for efficient free-coreductant gram-scale epoxidation of olefins with molecular oxygen, J. Organomet. Chem. 896 (2019) 59–69.

[21] M. Kazemnejadi, B. Mahmoudi, Z. Sharafi, M.A. Nasseri, A. Allahresani, M. Esmaeilpour, Copper coordinated-poly (α-amino acid) decorated on magnetite graphene oxide as an efficient heterogeneous magnetically recoverable catalyst for the selective synthesis of 5–and 1–substituted tetrazoles from various sources: a comparative study, Appl. Organomet. Chem. 34 (2020), e5273.

[22] M.K. Ahmed, S.F. Mansour, R. Al-Wafi, Nanofibrous scaffolds of ε-polyprolactone containing Sr/Se-hydroxyapatite/graphene oxide for tissue engineering applications, Biomed. Mater. 16 (2021), 045030.

[23] S. Priyadarsini, S. Mohanty, S. Mukherjee, S. Basu, M. Mishra, Graphene and graphene oxide as nanomaterials for medicine and biology application, J. Nanostruct. Chem. 8 (2018) 123–137.

[24] Y. Luo, H. Shen, Y. Fang, Y. Cao, J. Huang, M. Zhang, J. Dai, X. Shi, Z. Zhang, CVD growth of graphene on NiTi alloy for enhanced biological activity, ACS Appl. Mater. Interfaces 7 (2015) 19876–19881.

[25] H.S. Budi, M.J. Ansari, S.A. Jasim, W.K. Abdelbasset, D. Bokov, Y.F. Mustafa, M.A. A. Najm, M. Kazemnejadi, Preparation of antibacterial Gel/PCL nanofibers reinforced by dicalcium phosphate-modified graphene oxide with control release of clindamycin for possible application in bone tissue engineering, Inorg. Chem. Commun. 139 (2022) 109336–109350.

[26] N. Udomluck, W.G. Koh, D.J. Lim, H. Park, Recent developments in nanofiber fabrication and modification for bone tissue engineering, Int. J. Mol. Sci. 21 (2020) 99.

[27] M. Heidari, S.H. Bahrami, M. Ranjbar-Mohammadi, P.B. Milan, Smart electrospun nanofibers containing PCL/gelatin/graphene oxide for application in nerve tissue engineering, Mater. Sci. Eng. C 103 (2019), 109768.

[28] A. Fakhrali, N. Poursharifi, M. Nasari, D. Semnani, H. Salehi, M. Ghane, S. Mohammadi, Fabrication and characterization of PCL/Gel nanofibrous scaffolds incorporated with graphene oxide applicable in cardiac tissue engineering, Polym. Plast. Technol. Mater. 60 (2021) 2025–2041.

[29] S. Kashte, R.K. Sharma, S. Kadam, Layer-by-layer decorated herbal cell compatible scaffolds for bone tissue engineering: a synergistic effect of graphene oxide and Cissus quadrangularis, J. Bioact. Compat. Polym. 35 (2020) 57–73.

[30] G. Belgheisi, M.H. Nazarpak, M.S. Hashjin, Bone tissue engineering electrospun scaffolds based on layered double hydroxides with the ability to release vitamin D3: Fabrication, characterization and in vitro study, Appl. Clay Sci. 185 (2020), 105434.

[31] F. Panahi, R. Fareghi-Alamdari, S. Khajeh Dangolani, A. Khalafi-Nezhad, M. Golestanzadeh, Graphene grafted N-methyl-4–pyridinamine (G-NMPA): An efficient heterogeneous organocatalyst for acetylation of alcohols, ChemistrySelect 2 (2017) 474–479.

[32] S. Ilican, Y. Caglar, M. Caglar, F. Yakuphanoglu, Electrical conductivity, optical and structural properties of indium-doped ZnO nanofiber thin film deposited by spray pyrolysis method, Phys. E 35 (2006) 131–138.

[33] S. Chawla, M. Naraghi, A. Davoudi, Effect of twist and porosity on the electrical conductivity of carbon nanofiber yarns, Nanotechnology 24 (2013), 255708.

[34] Z.M. Goudarzi, T. Behzad, L. Ghasemi-Mobarakeh, M. Kharaziha, M.S. Enayati, Structural and mechanical properties of fibrous poly (caprolactone)/gelatin nanocomposite incorporated with cellulose nanofibers, Polym. Bull. 77 (2020) 717–740.

[35] D.W. Sheibley, L.L. Rieker, L.C. Hsu, M.A. Manzo, U.S. Pat., 1982, 4,357–402.

[36] Y. Wan, W. Huang, Z. Wang, X.X. Zhu, Preparation and characterization of high loading porous crosslinked poly (vinyl alcohol) resins, Polymer 45 (2004) 71–77.

[37] Z. Wang, J. Luo, X.X. Zhu, S. Jin, M.J. Tomaszewski, Functionalized cross-linked poly (vinyl alcohol) resins as reaction scavengers and as supports for solid-phase organic synthesis, J. Comb. Chem. 6 (2004) 961–966.

[38] A.C. Weems, M.C. Arno, W. Yu, R.T. Hucksteep, A.P. Dove, 4D polycarbonates *via* stereolithography as scaffolds for soft tissue repair, Nat. Commun. 12 (2021) 1–14.

[39] M. Şamlı, O. Bayraktar, F. Korel, Characterization of silk fibroin based films loaded with rutin–β-cyclodextrin inclusion complexes, J. Incl. Phenom. Macrocycl. Chem. 80 (2014) 37–49.

[40] T. Higashi, A. Tajima, K. Motoyama, H. Arima, Cyclodextrin/poly (ethylene glycol) polypseudorotaxane hydrogels as a promising sustained-release system for lysozyme, J. Pharm. Sci. 101 (2012) 2891–2899.

[41] J. Sun, R. Wang, M. Xia, S. Zhu, X.E. Zhao, Convenient and sensitive colorimetric determination of alendronate sodium with $Ce^{4+}$-triggered oxidation of TMB, New J. Chem. 44 (2020) 12962–12966.

[42] Q. Bao, H. Zhang, J.X. Yang, S. Wang, D.Y. Tang, R. Jose, R. Ramakrishna, C. T. Lim, K.P. Loh, Graphene–polymer nanofiber membrane for ultrafast photonics, Adv. Funct. Mater. 20 (2010) 782–791.

[43] S.T. Chen, E.M. Faller, K. Kobata, M.A. Fadli, C.S. Yeoh, Effect of collagen-related compound on cell proliferation and matrix production with cultured human dermal fibroblasts, Int. J. Med. Toxicol. Leg. Med. 21 (2018) 269–273.

[44] A.E. Wan, M.S.B. Khan, B.S.X. Teo, J. Khan, I. Abdullah, M. Kaleemullah, F. Asmani, M. Suofeiya, S. Al-Dhalli, Z. Kasim, S. Fattepur, Screening of antioxidant and antibacterial activity of methanolic extract of Ipomoea aquatica leaf and stem against bacteria causes skin infection, Int. J. Med. Toxicol. Leg. Med. 23 (2020) 169–178.

[45] S.H. Kim, H.S. Lee, D.S. Ryu, S.J. Choi, D.S. Lee, Antibacterial activity of silver-nanoparticles against Staphylococcus aureus and Escherichia coli, Microbiol, Biotechnol. Lett. 39 (2011) 77–85.

[46] S.S. Birla, V.V. Tiwari, A.K. Gade, A.P. Ingle, A.P. Yadav, M.K. Rai, Fabrication of silver nanoparticles by Phoma glomerata and its combined effect against Escherichia coli, Pseudomonas aeruginosa and Staphylococcus aureus, Lett. Appl. Microbiol. 48 (2009) 173–179.

[47] Z. Othman, H.R.H. Khalep, A.Z. Abidin, H. Hassan, S. Fattepur, The anti-angiogenic properties of morinda citrifolia. l (mengkudu) leaves using chicken chorioallantoic membrane (CAM) assay, Pharmacogn. J. 11 (2019) 12–15.

[48] S. Gao, W. Guo, M. Chen, Z. Yuan, M. Wang, Y. Zhang, S. Liu, T. Xi, Q. Guo, Fabrication and characterization of electrospun nanofibers composed of decellularized meniscus extracellular matrix and polycaprolactone for meniscus tissue engineering, J. Mater. Chem. B 5 (2017) 2273–2285.

[49] S.B. Thoke, Y.P. Sharma, S.S. Rawat, S.L. Nangude, Formulation development & evaluation of effervescent tablet of Alendronate sodium with vitamin D3, J. Drug Deliv. Ther. 3 (2013) 65–74.

[50] S. Deng, V. Berry, Wrinkled, rippled and crumpled graphene: an overview of formation mechanism, electronic properties, and applications, Mater. Today 19 (2016) 197–212.

[51] N. Le Moigne, M. van Den Oever, T. Budtova, Composites, A statistical analysis of fibre size and shape distribution after compounding in composites reinforced by natural fibres, Part A 42 (2011) 1542–1550.

[52] L. Dejob, B. Toury, S. Tadier, L. Grémillard, C. Gaillard, V. Salles, Electrospinning of in situ synthesized silica-based and calcium phosphate bioceramics for applications in bone tissue engineering: a review, Acta Biomater. 123 (2021) 123–153.

[53] N. Siddiqui, B. Kishori, S. Rao, M. Anjum, V. Hemanth, S. Das, E. Jabbari, Electrospun polycaprolactone fibres in bone tissue engineering: a review, Mol. Biotechnol. 63 (2021) 363–388.

[54] L. Jiang, D. Chen, Z. Wang, Z. Zhang, Y. Xia, H. Xue, Y. Liu, Preparation of an electrically conductive graphene oxide/chitosan scaffold for cardiac tissue engineering, Appl. Biochem. Biotechnol. 188 (2019) 952–964.

[55] B.D. Holt, Z.M. Wright, A.M. Arnold, S.A. Sydlik, Graphene oxide as a scaffold for bone regeneration, Wiley Interdiscip. Rev. Nanomed. Nanobiotechnol. 9 (2017), e1437.

[56] S. Ramazani, M. Karimi, Electrospinning of poly (ε-caprolactone) solutions containing graphene oxide: effects of graphene oxide content and oxidation level, Polym. Compos. 37 (2016) 131–140.

[57] F. Yener, O. Jirsak, Comparision of needle and roller electrospinning system of polyvinylbutyral, J. Nanomater. 2012 (2012), 839317.

[58] J.E. Oliveira, L.H. Mattoso, W.J. Orts, E.S. Medeiros, Structural and morphological characterization of micro and nanofibers produced by electrospinning and solution blow spinning: a comparative study, Adv. Mater. Sci. Eng. 2013 (2013).

[59] X. Chen, Y. Zhang, X. He, H. Li, B. Wei, W. Yang, Electrospinning on a plucked string, J. Mater. Sci. 54 (2019) 901–910.

[60] M.A. Dobrovolskaia, J.D. Clogston, B.W. Neun, J.B. Hall, A.K. Patri, S.E. McNeil, Method for analysis of nanoparticle hemolytic properties *in vitro*, Nano Lett. 8 (2008) 2180–2187.

[61] E.B. Nursanto, A. Nugroho, S.A. Hong, S.J. Kim, K.Y. Chung, J. Kim, Facile synthesis of reduced graphene oxide in supercritical alcohols and its lithium storage capacity, Green Chem. 13 (2011) 2714–2718.

[62] Y. Shen, T. Jing, W. Ren, J. Zhang, Z.G. Jiang, Z.Z. Yu, A. Dasari, Chemical and thermal reduction of graphene oxide and its electrically conductive polylactic acid nanocomposites, Compos. Sci. Technol. 72 (2012) 1430–1435.

[63] A. Abbasi, M.M. Nasef, M. Takeshi, R. Faridi-Majidi, Electrospinning of nylon-6, 6 solutions into nanofibers: rheology and morphology relationships, Chin. J. Polym. Sci. 32 (2014) 793–804.

[64] M. Heidari, H. Bahrami, M. Ranjbar-Mohammadi, Fabrication, optimization and characterization of electrospun poly (caprolactone)/gelatin/graphene nanofibrous mats, Mater. Sci. Eng. C 78 (2017) 218–229.

[65] S. Unal, S. Arslan, T. Gokce, B.M. Atasoy, B. Karademir, F.N. Oktar, O. Gunduz, Design and characterization of polycaprolactone-gelatin-graphene oxide scaffolds for drug influence on glioblastoma cells, Eur. Polym. J. 115 (2019) 157–165.

[66] C. Wan, B. Chen, Poly (ε-caprolactone)/graphene oxide biocomposites: mechanical properties and bioactivity, Biomed. Mater. 6 (6) (2011), 055010.

[67] S. Mahesh, K.C. Tang, M. Raj, Amide bond activation of biological molecules, Molecules 23 (2018) 2615.

[68] R. Huang, X. Chen, Y. Dong, X. Zhang, Y. Wei, Z. Yang, W. Li, Y. Guo, J. Liu, Z. Yang, H. Wang, L. Jin, MXene composite nanofibers for cell culture and tissue engineering, ACS Appl. Bio Mater. 3 (2020) 2125–2131.

[69] E. Tomecka, M. Wojasinski, E. Jastrzebska, M. Chudy, T. Ciach, Z. Brzozka, Poly (l-lactic acid) and polyurethane nanofibers fabricated by solution blow spinning as potential substrates for cardiac cell culture, Mater. Sci. Eng. C 75 (2017) 305–316.

[70] C. Baptista, A. Azagury, H. Shin, C.M. Baker, E. Ly, R. Lee, E. Mathiowitz, The effect of temperature and pressure on polycaprolactone morphology, Polymer 191 (2020), 122227.

[71] M. Sattary, M.T. Khorasani, M. Rafienia, H.S. Rozve, Incorporation of nanohydroxyapatite and vitamin D3 into electrospun PCL/Gelatin scaffolds: The influence on the physical and chemical properties and cell behavior for bone tissue engineering, Polym. Adv. Technol. 29 (2018) 451–462.

[72] S. Kumar, D. Azam, S. Raj, E. Kolanthai, K.S. Vasu, A.K. Sood, K. Chatterjee, 3D scaffold alters cellular response to graphene in a polymer composite for orthopedic applications, J. Biomed. Mater. Res. Part B 104 (2016) 732–749.

[73] P.N. Christy, S.K. Basha, V.S. Kumari, A.K.H. Bashir, M. Maaza, K. Kaviyarasu, M. V. Arasu, N.A. Al-Dhabi, S. Ignacimuthu, Biopolymeric nanocomposite scaffolds for bone tissue engineering applications–a review, J. Drug Deliv. Sci. Technol. 55 (2020), 101452.

[74] A. Shahini, M. Yazdimamaghani, K. Walker, M. Eastman, H. Hatami-Marbini, B. Smith, J. Ricci, S. Madihally, D. Vashaee, L. Tayebi, 3D conductive nanocomposite scaffold for bone tissue engineering, Int. J. Nanomed. 9 (2014) 167–181.

[75] S. Shao, S. Zhou, L. Li, J. Li, C. Luo, J. Wang, X. Li, J. Weng, Osteoblast function on electrically conductive electrospun PLA/MWCNTs nanofibers, Biomaterials 32 (2011) 2821–2833.

[76] A.G. Guex, J.L. Puetzer, A. Armgarth, E. Littmann, E. Stavrinidou, E.P. Giannelis, G.G. Malliaras, M.M. Stevens, Highly porous scaffolds of PEDOT: PSS for bone tissue engineering, Acta Biomater. 62 (2017) 91–101.

[77] M.T.H. Aunkor, T. Raihan, S.H. Prodhan, H.S.C. Metselaar, S.U.F. Malik, A.K. Azad, Antibacterial activity of graphene oxide nanosheet against multidrug resistant superbugs isolated from infected patient, R. Soc. Open Sci. 7 (2020), 200640.

[78] H. Mohammed, A. Kumar, E. Bekyarova, Y. Al-Hadeethi, X. Zhang, M. Chen, M. S. Ansari, A. Cochis, L. Rimondini, Antimicrobial mechanisms and effectiveness of graphene and graphene-functionalized biomaterials. a scope review, Front. Bioeng. Biotechnol. 8 (2020) 465.

[79] R. Mann, D. Mitsidis, Z. Xie, O. McNeilly, Y.H. Ng, R. Amal, C. Gunawan, Antibacterial activity of reduced graphene oxide, J. Nanomater. 2021 (2021) 9941577.

[80] Y.H. Yu, C.C. Chan, Y.C. Lai, Y.Y. Lin, Y.C. Huang, W.F. Chi, C.W. Kuo, H.M. Lin, P. C. Chen, Biocompatible electrospinning poly (vinyl alcohol) nanofibres embedded with graphene-based derivatives with enhanced conductivity, mechanical strength and thermal stability, RSC Adv. 4 (2014) 56373–56384.

[81] S. Sayyar, E. Murray, B.C. Thompson, S. Gambhir, D.L. Officer, G.G. Wallace, Covalently linked biocompatible graphene/polycaprolactone composites for tissue engineering, Carbon 52 (2013) 296–304.

[82] H. Ma, W. Su, Z. Tai, D. Sun, X. Yan, B. Liu, Q. Xue, Preparation and cytocompatibility of polylactic acid/hydroxyapatite/graphene oxide nanocomposite fibrous membrane, Chin. Sci. Bull. 57 (2012) 3051.